Remote Sensing Applications: Society and Environment 29 (2023) 100921

Contents lists available at ScienceDirect

Remote Sensing Applications: Society and Environment

journal homepage: www.elsevier.com/locate/rsase

Thermal infrared remote sensing data downscaling investigations: An overview on current status and perspectives

Ruiliang Pu [a], Stefania Bonafoni [b, *]

[a] University of South Florida, Tampa, FL 33620, USA
[b] Department of Engineering, University of Perugia, 06125, Perugia, Italy

ARTICLE INFO

Keywords:
Thermal infrared (TIR) remote sensing
Land surface temperature (LST)
Disaggregation of LST
Downscaling LST (DLST)

ABSTRACT

Land surface temperature (LST) retrieved from moderate resolution or downscaled from coarse thermal infrared (TIR) data is one of key environment parameters. Over the last four decades, most advanced remote sensing sensors/systems can acquire TIR data at a low spatial resolution but high temporal resolution. However, per different application purposes, both high spatial and temporal resolution TIR data are needed. Given that many investigations on downscaling LST (DLST) processes have been done and findings have been reported in the literature, it necessitates to have an updated review on DLST investigations of the status, trends, and challenges and to recommend future directions. An overview is provided on various polar orbits and geostationary orbits' satellite TIR sensors/systems and on scaling factors' determination and selection techniques/methods suitable for DLST processes. Existing various techniques/methods for DLST processes are presented and assessed, and limitations and future research directions are identified and recommended. In this review, several concluding remarks were made, including (1) most investigations on DLST processes used coarse spatial resolution but high temporal resolution MODIS TIR data; (2) compared to fusion-based method, the kernel-driven processes are the most frequently used thermal downscaling methods; (3) machine-learning methods have demonstrated their excellent performance and robustness in improving DLST accuracy; (4) more advanced spatiotemporal fusion-based methods consider synergic powers by combining a kernel-driven process with a fusion-based process method. The three future research directions for DLST processes are recommended: further reducing uncertainties of DLST results, developing novel DLST models and algorithms, and directly reducing the spatial scaling effect in DLST processes.

1. Introduction

1.1. Significance of high resolution thermal remote sensing data

Thermal infrared (TIR) remote sensing, covering TIR range 3–12 μm (typical 8–14 μm), can be acquired by electro-optical sensors in either a single broadband or multispectral or even hyperspectral images. Land surface temperature (LST) retrieved from remote sensing TIR data is a key environmental parameters at local, regional to global scales (Zhan et al., 2013; Mao et al., 2021). Usually, coarse remote sensing sensors/systems can acquire TIR data at a low spatial resolution but high temporal resolution compared to optical (visible-near infrared (VNIR) and short-wave infrared (SWIR)) data. Due to the issue of the trade-off between spatial and temporal resolutions in modern thermal remote sensing technologies, it is extremely difficult to acquire both high temporal and spatial resolu-

* Corresponding author.
E-mail addresses: rpu@usf.edu (R. Pu), stefania.bonafoni@unipg.it (S. Bonafoni).

https://doi.org/10.1016/j.rsase.2023.100921
Received 2 December 2022; Received in revised form 26 December 2022; Accepted 10 January 2023
Available online 18 January 2023

tions TIR imagery (Zhan et al., 2013; Xia et al., 2019; Mao et al., 2021). Given that LST plays a valuable role in controlling environmental, physical, ecological, and biological processes (Wan and Dozier, 1996; Zhan et al., 2013; Xia et al., 2019), it is desirable to have LST data at both high spatial (i.e., tens of meters or even a few meters) and high temporal resolutions for many application purposes, such as mapping surface evapotranspiration in agricultural and arid regions (Anderson et al., 2012; Bindhu et al., 2013; Olivera-Guerra et al., 2017; Liu et al., 2018b), studying urban thermal environments (Stathopoulou and Cartalis, 2009; Sobrino et al., 2012; Zakšek and Oštir, 2012; Wang et al., 2020b) and urban heat island (UHI) effects (Zhou et al., 2019), and characterizing urban heterogenous landscapes (Bonafoni et al., 2016; Bonafoni, 2016; Yang et al., 2019; Zawadzka et al., 2020).

To overcome the dilemma (i.e., low spatial resolution but high temporal resolution) of most available satellite TIR remote sensing sensors, during the last four decades, a lot of studies have conducted to investigate downscaling LST (DLST) processes (from a relatively lower/coarser spatial resolution to a relatively finer resolution) to generate high spatial LST data to meet many application purposes. Such investigations of DLST techniques/methods of coarse TIR data have attracted the interest of a lot of researchers. Sequentially, there are more and more research projects/studies that have been done and their analysis results and novel findings were reported in the currently literature (Fig. 1). To outline current status and point future direction and promote the research and application of DLST techniques and methods as well, some review papers have been published. Table 1 lists and summarizes the topics and objectives of three existing review papers that are closely related to this review for downscaling LST from a coarse resolution to finer resolutions. Compared to the major issues or contents/components reviewed in the three papers (Table 1), in this review paper, (1) an update of review including newly published studies; (2) more detailed and update TIR remote sensing sensors/systems are presented; (3) more comprehensive and detailed state-of-the-art DLST techniques and methods are reviewed and assessed; and (4) more specific future research directions are pointed out (e.g., novel and optimized DLST models and algorithms, direct reduction of scaling effects in DLST). Concerning point 3, we considered a) an overview of reference data (field and image based); b) a comprehensive analysis of the scaling factors (characteristics and selection); c) the analysis of different methods: classic-based, regression-based, machine learning-based, TIR spectral unmixing-based, spatiotemporal fusion-based; d) an insight on the spatial scaling effects and reduction approaches.

In general, DLST processes can provide a better resolutions dataset of LST at both finer spatial and temporal resolutions and thus it is widely thought as an effective tool to utilize subpixel thermal energy for many applications. In current literature, the relevant studies on DLST techniques/methods have used different terms from DLST but have the same or similar meaning, which include fre-

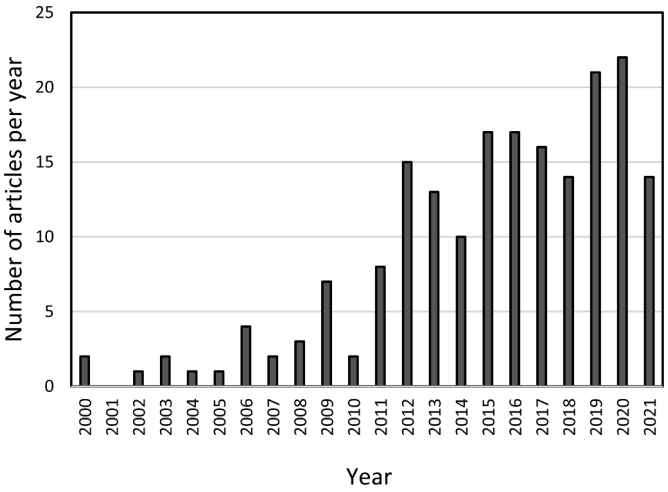

Fig. 1. Number of papers published related to DLST processes after 2000.

Table 1
Summary of focuses/objectives of major existed review papers related to DLST.

Authors (year)	Title	Focus/objective
Zhan et al. (2013)	Disaggregation of remotely sensed land surface temperature: Literature survey, taxonomy, issues, and caveats	Overview on DLST: various assumptions, terms/definition, categories, their relationships, illustrations, advantages/disadvantages/limitations, etc. This review gives a generalization of thermal sharpening (TSP) and temperature unmixing (TUM), promotes the understanding of DLST, suggests future research.
Yoo et al. (2020)	Spatial downscaling of MODIS land surface temperature: Recent research trends, challenges, and future directions	A comprehensive overview on current research trends for downscaling MODIS LST based on a recent literature survey covering past decade. Techniques classified into three groups—kernel-driven, fusion-based, and the combination of both methods. Future research directions are pointed out.
Mao et al. (2021)	Resolution enhancement of remotely sensed land surface temperature: Current status and perspectives	Review on the current status of DLST data; comprehensive investigation and analysis of three groups of DLST methods: spatial or temporal resolution enhancements, or simultaneous spatiotemporal resolution enhancement. Key directions for future studies of DLST.

quently used: disaggregation of LST, spatial resolution improvement of LST, spatial enhancement of LST, spatial (thermal) sharpening, subpixel temperature estimation, thermal spectral unmixing, component temperature retrieval. In this review, DLST will be a representative term for all of them even though the various terms may be directly cited in specific studies reviewed in this paper.

1.2. Review objectives

In this review, an overview is provided on TIR remote sensing data downscaling investigations, especially reviewing and assessing the state-of-the-art techniques and methods of DLST and spatial scaling effect in DLST processes. The substantial objectives of this paper are to.

- review high temporal resolution but low spatial resolution TIR sensors and systems frequently used for coarse resolution TIR data spatial sharpening and spectral unmixing studies;
- provide an overview on, and characterize, different techniques/methods for downscaling LST from coarse/native resolutions to finer target resolutions;
- Assess spatial scaling effect on DLST results and review approaches to measure and reduce the scaling effects on DLSTs; and
- Identify limitations and constraints existing in current DLST processes and point future research directions for improving DLST results and promoting applications of TIR remote sensing at finer resolutions in different areas.

1.3. Review approach

In this review of DLST with various coarse resolution TIR remote sensing sensors/systems' data, a total of 220 peer-review journal and proceedings papers in English language were reviewed, but among them, only 135 papers were directly cited in this review (remaining 85 papers have also been involved in some figures). Although a few of DLST related journal papers published before 2000 were included in the list for this project, this review is more emphasizing papers published in and after 2000, especially after 2010. The Web of Science (https://www.webofscience.com/wos/woscc/basic-search) was accessed for searching for relevant papers published during the last four decades based on the following terms in Topic: [(thermal sharpening AND LST) OR (subpixel temperature estimation AND LST) OR downscaling LST OR (component temperature retrieval AND LST) OR spatial enhancement of LST OR spatial resolution improvement of LST OR (thermal fusion AND LST) OR disaggregation of LST OR ((temperature unmixing AND LST) OR (temperature mixture analysis AND LST)) OR super-resolution of LST]. There were about 570 studies on the topic to be found. Then the 570 studies were further screened by referring to the following criteria all met to form a final list (216) of papers reviewed for this project.

- A study reported in a paper must downscale TIR data from a coarse/native resolution to at least one finer spatial resolution;
- A study must generate and/or present DLST results in a form of table and/or figure;
- A study must investigate effect(s) of scaling factors or kernel set (type and characteristics) and/or (&) technique/methods of DLST & temporal & data pre-processing & feature extraction methods on DLST results;
- A study must present detailed accuracy assessment results of TIR data downscaling processes.

In this review, after discussing the significance and importance of high resolutions (spatial and temporal) TIR data in land surface processes, review objectives and approach, a full list of modern TIR remote sensing sensors/systems frequently used in downscaling processes, including geostationary orbit, polar orbit satellite TIR remote sensing sensors/systems, is reviewed. Next, methods and techniques for downscaling TIR data are reviewed and assessed with a particular interest in reference data collection, scaling factors (kernels) extraction and selection, DLST processing methods and algorithms and their characteristics. As a challenge in downscaling TIR data processes, the spatial scaling effect is evaluated and possible approaches to measure and correct the effect are discussed. Finally, after identifying and discussing current limitations and constraints of techniques and methods for downscaling TIR data, possible future research directions for improving DLST results are pointed out.

2. Satellite TIR remote sensing sensors/systems

Satellite TIR remote sensing sensors' data that are currently available for downscaling processes include a moderate to coarse spatial resolution and 35 days to 15 min temporal resolution (Table 2). The platforms of modern TIR remote sensing sensors/systems consist of different polar orbits and geostationary obits. Table 2 summarizes TIR remote sensing sensors/systems currently used for DLST processes from sensors' name and characteristics including band setting and information sources, etc. Fig. 2 presents TIR sensors that are frequently used for DLST processes, calculated from the list of papers/studies reviewed in this study.

2.1. Polar orbits (I): moderate resolution TIR sensors

Moderate resolution satellite TIR sensors currently used for DLST processes include those onboard Landsat series and Terra with spatial resolution better a few 100 m. The Thematic Mapper (TM) onboard Landsat 4/5, the Enhanced Thematic Mapper Plus (ETM+) onboard Landsat 7, and the Thermal Infrared Sensor (TIRS) onboard Landsat 8 measure land surface thermal energy in one or two thermal bands, while the Advanced Spaceborne Thermal Emission and Reflection Radiometer (ASTER) sensor carried by Terra satellite senses land surface TIR energy in five multispectral thermal bands (Table 2). Recent years, many DLST processing studies (Fig. 2) have indicated that the Landsat series sensors and ASTER TIR data have been popularly used for DLST processes to create high (e.g., 30 m resolution) and very high (better than 30 m resolution, VHR) (e.g., Jiang and Weng, 2013; Pu, 2021), and, coupling some coarse spatial resolution but high temporal TIR sensors (e.g., Moderate Resolution Imaging Spectroradiometer (MODIS)), high spatiotemporal Landsat-like time series TIR data (e.g., Herrero-Huerta et al., 2019; Yao et al., 2020). For example, Jiang and Weng

Table 2
A list of moderate - coarse spatial but high temporal resolution thermal remote sensing sensors/systems frequently used for downscaling LST processes.

Satellite	Sensor/ system	Revisit period[a]	No. of TIR bands	TIR spectral range, wavelength (μm)	Spatial resolution (m)	Operation	Information source[b]
Polar orbits (I): Moderate resolution (pixel size < 1000 m)							
Landsat-4,-5	TM	16 D	1	10.4–12.5	120	1982–2011	https://earthexplorer.usgs.gov/
Landsat-7	ETM+	16 D	1	10.4–12.5	60	Since 1999	https://earthexplorer.usgs.gov/
Landsat-8	TIRS	16 D	2	10.60–11.19, 11.50–12.51	100	Since 2013	https://earthexplorer.usgs.gov/
Terra	ASTER	on-demand	5	8.125–8.475, 8.475–8.825, 8.925–9.275,10.25–10.95, 10.95–11.65	90	Since 1999	https://earthexplorer.usgs.gov/
Polar orbits (II): Coarse resolution (pixel size ≥ 1000 m)							
Terra/Aqua	MODIS	1 - 2 D	2	10.78–11.28, 11.77–12.27	1000	Since 1999	https://modis.gsfc.nasa.gov/
NOAA	AVHRR	0.5 D	2	10.5–11.3, 11.5–12.5	1100	Since 1979	https://www.avl.class.noaa.gov/release/data_available/avhrr/index.htm
Envisat	AATSR	35 D	2	11.0, 12.0	1000	Since 2002	http://www.atsrsensors.org/aatsr.htm
ERS	ATSR	35 D	2	11.0, 12.0	1000	Since 1991	http://www.atsrsensors.org/aboutATSR.htm
Sentinel-3(A/B)	SLSTR	1 D	2	10.85, 12.02	1000	Since 2016	https://sentinel.esa.int/web/sentinel/home
Fengyun-3(A/B/C)	VIRR	5.5 D	2	10.3–11.3, 11.5–12.5	1100	Since 2008	https://fy4.nsmc.org.cn/data/en/instrument/VIRR.html
Geostationary orbits							
GOES	Imager	3 H	2	10.2–11.2.11.5–12.5	4000	Since 1975	https://www.goes.noaa.gov/
Meteosat-8, MSG	SEVIRI	15 M	2	9.8–11.8, 11.0–13.0	3000	Since 2005	https://www.eumetsat.int/seviri
INSAT	VHRR	<1 D	1	10.5–12.5	8000	Since 2003	https://www.mosdac.gov.in/insat-3a
Fengyun-4A	AGRI	15 M	4	8.0–9.0, 10.3–11.3, 11.5–12.5, 13.2–13.8	4000	Since 2016	https://fy4.nsmc.org.cn/nsmc/en/theme/FY4A_instrument.html

Note.
[a] D-day, H-hour, M-minute (limited in the table).
[b] Accessed on November 14, 2021.

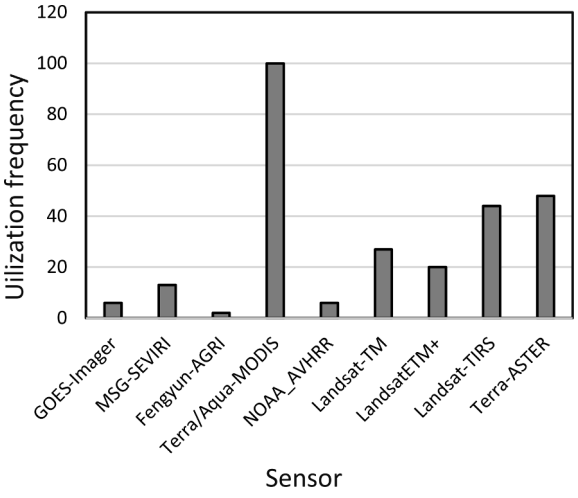

Fig. 2. Utilization frequency of moderate - coarse spatial but high temporal resolution TIR remote sensing sensors/systems.

(2013) downscaled Landsat TM 120 m LST to 30 m fine resolution by using a vegetation cover-based thermal sharpening method. Bonafoni et al. (2016) conducted downscaling Landsat LST over the urban area of Florence, Italy from a native 120 resolution to 30 fine resolution with TM optical data derived scaling factors. Essa et al. (2012) downscaled ETM+ 60 LST to 30 m resolution with 15 spectral indies as scaling factors. Zawadzka et al. (2020) proposed a DLST method for downscaling Landsat 8 TIRS derived 100 m resolution LST to 2–4 m by using scaling factors extracted from very high resolution hyperspectral aerial imagery and large-scale topographic maps. In assessing scaling effect in DLST processes at different at high and very high spatial resolutions, Pu (2021) conducted

downscaling ASTER 90 m resolution LST to 4–30 m finer spatial resolutions. In addition, Herrero-Huerta et al. (2019) and Yao et al. (2020) downscaled TM/TIRS 120 m and 100 m LSTs coupled with MODIS 1000 m LST to create high spatiotemporal Landsat-like 30 m resolution time series LSTs. There are many other similar studies on downscaling the moderate resolution TIR sensors' data to high and very high resolutions including, but not limited to, DLSTs from TM 120 m to finer resolutions by Tom et al. (1985) and Guo et al. (2014); from ETM+ 60 m to finer resolutions by Deng and Wu (2013a); from TIRS 100 m to finer resolutions by Wang et al. (2017); from ASTER 90 m LST to finer resolutions by Gustafson et al. (2003), Xu et al. (2020), Hu et al. (2021), and Zhou and Zhang (2021).

Given the fact that the moderate resolution TIR sensors' data can be downscaled to high and VHR resolutions, most of the DLSTs downscaled from the TIR sensors' data are used for mapping and characterizing thermal environments with heterogenous landscapes, such as heterogenous urban landscapes. For example, Huang et al. (2013) and Yao et al. (2020) utilized DLSTs at high resolutions, downscaled from the Landsat TIR sensors' LST to characterize and monitor UHIs. Zawadzka et al. (2020) generated the VHR DLSTs for characterizing heterogenous urban landscapes.

2.2. Polar orbits (II): coarse resolution TIR sensors

Typical high temporal resolution (0.5–2 days) but low spatial resolution (~1000 m) sensors/systems, popularly used for DLST processes, specify the NASA-MODIS sensor onboard the Terra/Aqua satellites and the NOAA-AVHRR (Advanced Very High-Resolution Radiometer). Other polar orbits coarse resolution TIR sensors with less investigation for DLST processes also include the European Space Agency's Along-Track Scanning Radiometer (ATSR), Advanced ATSR (AATSR), and the Sea and Land Surface Temperature Radiometer (SLSTR) onboard Sentinel-3(A/B) and the Visible and Infrared Radiometer (VIRR) onboard Fengyun-3 (B/C) (Table 2). The coarse resolution TIR sensors' data can be used for downscale to different moderate resolutions (mostly a few 100 m). In the current literature, it is easily found that there are a lot of studies on DLST processes with the coarse resolution TIR sensors' data, especially the MODIS coarse resolution LST data (Fig. 2), for which, researchers either directly used real MODIS LST data to downscale to moderate resolutions or used MODIS-like LST data simulated by aggregating moderate resolution sensors' data to downscale. For example, Mukherjee et al. (2014) used the original 1000 m MODIS LST data to downscale to 250 m LST and the Landsat TM upscaled 960 m LST data to downscale to 480 m and 240 m LSTs over heterogeneous landscapes. Sharma et al. (2020) also utilized both real MODIS 1000 m LST data and aggregated Landsat 8 LST data at 1000 m resolution to downscale to 400, 300, 200, and 100 m resolutions. In addition, to create high spatiotemporal time series TIR data, the coarse resolution MODIS data are coupled with moderate resolution sensors (e.g., TM, TIRS and ASTER) by using spatiotemporal-based models (discussing them in section 3.3 below). For instance, Moosavi et al. (2015) fused multitemporal MODIS and Landsat TIRS TIR data to predict daily LST at 100 m-resolution. To monitor an environmental process, Wu et al. (2015) generated daily high spatial resolution LSTs by fusing ASTER and MODIS LST products. There were some studies on downscaling other coarse resolution TIR sensors' data to moderate resolutions, including AVHRR (e.g., Matson and Dozier, 1981; Stathopoulou and Cartalis, 2009; Chybicki and Łubniewski, 2017).

The moderate resolution LSTs downscaled from the coarse resolution TIR sensors are mostly used for mapping, monitoring and characterizing large landscapes and some cases at a regional scale. For example, such DLSTs from the coarse TIR sensors' data were used to map and monitor soil moisture (e.g., Amazirh et al., 2019; Bai et al., 2019), agriculture landscapes (e.g., Jeganathan et al., 2011; Mukherjee et al., 2015; Eswar et al., 2016), and evapotranspiration (e.g., Bindhu et al., 2013; Bisquert et al., 2016; Mahour et al., 2017; Olivera-Guerra et al., 2017; Liu et al., 2018b).

2.3. Geostationary orbits TIR sensors

Geostationary orbits TIR sensors can provide TIR image data within the same region (dish area) of the Earth at high temporal resolution (e.g., 15 min) (Mao et al., 2021). They include Imager onboard GOES (Geostationary Operational Environmental Satellite), SEVIRI onboard MSG (Meteosat Second Generation), and AGRI onboard Fengyun-4A, etc. They are currently used for LST downscaling from very coarse native spatial resolution (a few of kilometers but very high temporal resolution) to general coarse and moderate resolution LSTs (most in time series). Detailed information on commonly used geostationary orbits TIR sensors in LST downscaling processes are summarized in Table 2. There were many studies on DLST processes to generate MODIS-like spatial resolution LSTs for monitoring the Earth surface thermal budget including urban thermal environments. The DLSTs disaggregated from geostationary orbits TIR sensors are mostly at high temporal resolutions up to 15 min and cover regional or continental areas (e.g., SEVIRI covering most European and GOES-East most South and North Americans' areas). For example, Weng and Fu (2014) downscaled GOES Image 4 km LST to 1 km resolution to create a time series LST products for monitoring of UHI in the Los Angeles region by extracting and using key diurnal temperature cycle parameters. Jiang et al. (2015) used the disaggregated GOES Image LST data to MODIS-like 1 km resolution LSTS for assessing heat wave health risks at a regional scale. To create time series LST data for performing an urban heat island diurnal cycle analysis, Zakšek and Oštir (2012) downscaled SEVIRI onboard MSG LST data with 3 km × 5 km–1 km spatial resolution and 15 min temporal resolution LSTs. Sismanidis et al. (2017) also disaggregated ~4 km SEVIRI LST DLST to 1 km MODIS-like LST data to create a diurnal LST product. There are more studies on aggregating geostationary orbits TIR sensors' data to regular coarse (~1 km) and moderate resolution LST data (a few of 100 m) during the last two decades, including GOES TIR data (e.g., Kustas et al., 2003; Agam et al., 2007; Inamdar and French, 2009; Vaculik et al., 2019); MSG- SEVIRI TIR data (e.g., Zakšek and Schroedter-Homscheidt, 2009; Bechtel et al., 2012; Kallel et al., 2013; Mechri et al., 2014; Mechri et al., 2016; Njuki et al., 2020), and Fenyen-4A/SGRI TIR data (e.g., Zhu et al., 2018b).

3. Techniques and methods of downscaling LST

3.1. Reference data

To assess the performance of a new method/technique to downscale coarse resolution TIR sensors' data to finer resolutions, reference data are necessary for evaluating quality and accuracy of DLST results. According to different reference data sources, there are two approaches that can be adopted to collect the reference data, field-based (in-situ, UAV-based LST and TIR radiance measurements) approach and TIR/LST image-based approach. In addition, simulated data can be also used as the reference data that allow us to evaluate the strengths and weaknesses of a DLST method in some aspects (Quan et al., 2018; Xia et al., 2019b; Mao et al., 2021). However, since less studies with the simulated data as reference data are reported in the relevant literature, they were not reviewed in this paper.

3.1.1. Field (in-situ)-based approach

Based on requirements for assessing the performance of a new downscaling method and validating its DLST results, sampling methods (a random or systematic or typical sampling method) and samples (usually a set of plots distributed in areas of different land use/cover types) are first selected and deployed in a project area, then a set of in-situ samples of LST/TIR radiance are measured by adopting one field LST/TIR radiance measurement approach and required instrument (e.g., Coll et al., 2005; White-Newsome et al., 2013; Bonafoni et al., 2016). In practice, the field collected reference data are usually used for verifying DLST results at a high or very high resolution (e.g., better than 15 m) and a local scale (i.e., covering a relatively small study area), and thus the field-based approach is not suitable for validating DLST results covering a large or a regional area. For example, Zhou et al. (2016) downscaled ASTER 90 m LST data to 15 m high resolution and Landsat TIRS 100 m LST data to 30 m resolution. The DLST results were verified with field-measured LST data. To validate the DLST results at very high resolution (2 m) from upscaled moderate resolutions (40 m, 30 m, and 20 m), Bonafoni and Tosi (2017) first verified the retrieved LST from 2 m resolution airborne TIR data with the ground-measured LST data, then used the verified LST image to validate the DLST results. In recent years, a flexible UAV-carried sensors (LST thermometer or TIR radiometer) may be used for collecting the reference (imaging) data of LST/TIR radiance for DLST validation purpose (e.g., Wang et al., 2020).

Field LST measurements do not frequently necessarily represent LST values over a pixel area due to large spatial variations of LST at a pixel scale, depending on the pixel size (spatial resolution) and thermal spatial variation within the pixel area and on spatial heterogeneity of landscapes within the pixel area. This is because natural land cover materials and types and their corresponding LST and LSE (land surface emissivity) values are quite variable at scales of a few of 100 m^2 or of km^2 (Li et al., 2013). Homogeneous and flat Earth surfaces, such as inland water, sand, snow, and ice, which can be relatively easily measured and characterized, can serve as validation sites/areas (Snyder et al., 1997; Sobrino and Romaguera, 2004b; Coll et al., 2005; Guillevic et al., 2012). Thus, the field-based approach might not suitable for validating DLST results covering heterogenous surface and variable terrain areas, especially with a large pixel size.

3.1.2. Image-based approach

In LST/TIR data downscaling processes, the use of the image-based approach for assessing the DLST methods and validating DLST results perhaps is of one most popular and effective approach. This is because (i) the TIR/LST images, including airborne or satellite sensors' images, frequently have the same spatial or temporal or both spatiotemporal characteristics as those DLST results, and (ii) the most of moderate to coarse resolution TIR/LST images are easy to access and available for most users. Therefore, not like the field-based approach, verifying DLST results covering in a heterogenous and variable terrain surface and at moderate to coarse resolutions is reliable and accurate with the image-based approach via comparing the DLST results with appropriate scales/resolutions (spatial and temporal) images. To fit the spatial/temporal resolutions of DLST results, if the spatial/temporal resolutions of the images used for validating the DLSTs do not match those of DLST results, the images for validation purposes can be upscaled to the required resolutions for validating the DLST results. For example, Zhang et al. (2019) and Li et al. (2018) downscaled 1000 m or 990 m resolution MODIS LST to 90 m resolution LST, then validated the DLSTs at 90 m resolution with ASTER 90 m resolution LST product. Wang et al. (2020) and Luo et al. (2021) also disaggregated 1000 m resolution MODIS LST to 100 m resolution LST then validated the DLST at 100 m resolution with Landsat 8 TIRS 100 m LST data. Stathopoulou and Cartalis (2009) downscaled 1000 m resolution AVHRR data to 120 m DLST and validated with Landsat 120 m resolution TM LST. Jeganathan et al. (2011) first downscaled MODIS 1 km LST product to 810 m, …, and 180 m resolutions, then upscaled ASTER 90 m LST products to Dusts corresponding resolutions LSTs to verify the DLSTs from MODIS. When the acquisition time for the images for validation purposes is different from that for the coarse resolution LST image, it is necessary for the former images to normalize the possible LST difference caused by the time difference of acquiring images by adopting some normalization approaches (e.g., one introduced in Pu, 2021).

To test a newly developed DLST method/technique, many studies use upscaled (aggregated) TIR or LST data at lower resolutions to downscale to different finer resolution DLSTs then validate them with corresponding upscaled TIR or LST data. For example, Chen et al. (2014) first upscaled ASTER 90 m LST to 720 m resolution then downscaled to 90 m resolution LST and validated it with ASTER 90 m LST. Liu et al. (2018) first aggregated ETM+ 60 m LST to 960 m, 240 m, and 120 m for site 1 (an agriculture area) and TM 120 m LST to 960 m for site 2 (an urban area) then disaggregated to 240 m, 120 m, and 60 m for site 1 and to 480 m, 240 m, and 120 m for site 2. They validated the DLSTs at different resolutions with corresponding resolution upscaled ETM + LSTs from 60 m and TM LSTs from 120 m, respectively. There are a lot of other studies using upscaled lower resolution LSTs to downscale to different finer resolution LSTs with DLST methods and then validate them with corresponding upscaled LSTs, such as, using Landsat 8 TIRS LST by Xia et al. (2018) and Liang et al. (2021) and ASTER LST by Sattari et al. (2018). With the same sensor's data for testing and validat-

ing downscaling processes, one unique advantage is that DLST data and the images for a validation purpose have an identical image acquisition time.

3.2. Types and selection of scaling factors

Scaling factors (SFs), used as independent variables for kernel-based DLST processes, are extracted from relatively high resolution multi-/hyper-spectral optical sensors' data, mostly covering visible, NIR and MIR spectral ranges, and also from no-remote sensing ancillary data (e.g., DEM data). In the relevant DLST processes literature, there are many different terms but with the same meaning and/or function as SFs, frequently including kernels, predictors, independent variables, and explanatory variables, etc. Although different terms have be used in different studies, in this review, the SF is adopted.

3.2.1. Types and characteristics of SFs

In the kernel-based DLST processes, there are five types of SFs frequently seen in the literature, including (1) original spectral bands, (2) spectral (vegetation) indices, (3) land use land cover (LULC) types or their fraction images, (4) surface thermal related indices, and (5) terrain surface indices. Table 3 summarizes characteristics and references of the five types of SFs. Selected spectral band images in digital number or reflectance may directly be used as SFs for downscaling LST processes. There are some studies on DLST processes that directly used original spectral bands selected from optical bands as SFs, such as selecting original spectral bands from multispectral imagery by Tom et al. (1985), Li et al. (2018), Zhan et al. (2011), Hutengs and Vohland (2016) and from hyperspectral imagery by Ghosh and Joshi (2014).

In the kernel-based DLST processes, various spectral indices or vegetation indices (SIs or VIs) are commonly used as SFs. The SIs (VIs) are constructed with two to four typical blue, green, red, NIR and SWIR 1 (~1.6 μm) and SWIR 2 (~2.2 μm) bands selected from multi-/hyper-spectral imagery (Table 4). Table 4 presents a summary of 15 SIs frequently used as SFs in the most DLST processes, including their definitions (formulas), functions/characteristics and references. The physical characteristics of most SIs are related to surface features, such as biomass, vegetation cover, soil moisture and impervious area, which directly or indirectly denote surface thermal characteristics. Compared with directly using original spectral original bands, benefits of using these SIs may include easy to use and more enabling to denote surface thermal characteristics and thus to reflect spatiotemporal variation of LST. Therefore, SIs (e.g., NDVI) were used in some early classic DLST methods (e.g., DisTrad and TsHARP) and more recent studies have used different SIs (Table 4) as SFs in the kernel-based DLST techniques and methods. For example, Guo et al. (2014) and Lillo-Saavedra et al. (2018) used Landsat TM/TIRS LST data directly to downscale to finer resolution LST with their optical multispectral data derived SIs and other SFs. Eswar et al. (2016), Wu et al. (2019), and Bala et al. (2020) used Landsat ETM + and TIRS LST data first to upscale to lower resolution LSTs and then to downscale to finer resolution LSTs with SIs and other SFs extracted from Landsat optical multispectral

Table 3
Summary of types and characteristics of different scaling factors (kernels).

Type of scaling factors	Scaling factor (SF)	Characteristic & description	Reference
Spectral band	Spectral band	Spectral bands in digital number or reflectance are directly selected from multi-/hyper-spectral optical sensors.	Tom et al. (1985); Ghosh and Joshi (2014); Li et al. (2018).
Spectral Index (SI)	Spectral index	Using 2 or more multi-/hyper-spectra bands to construct a ratio or normalized difference ratio, or other SIs by an arithmetic operation. See Table 4 for list of SIs frequently used for scaling factors.	Pu (2021); Mao et al. (2021).
LULC type or its Fraction	Fraction of vegetation cover (Fvc)	A vegetation canopy cover within a pixel area in percentage (%) or [0, 1], frequently created with NDVI (e.g., Fvc = (NDVI - $NDVI_{min}$)/($NDVI_{max}$ - $NDVI_{min}$) or Fvc = 1 - (($NDVI_{max}$-NDVI)/($NDVI_{max}$-$NDVI_{min}$))$^{0.625}$).	Agam et al. (2007); Bisquert et al., 2016; Amazirh et al. (2019).
	Fraction (abundance) of endmembers (or LULC types)	Using spectral unmixing methods to create fraction/abundances of endmembers or LULC types. Using some supervised classifiers to created rule images (similar to fractions) of endmembers or LULC types.	Gustafson et al. (2003); Deng and Wu (2013b); Bonafoni and Tosi (2017); Pu (2021).
	LULC type	Using supervised classifiers to create LULC types from high resolution optical multi-/hyper-sensors' data.	Yang et al. (2011); Sismanidis et al. (2016); Li et al. (2019); Wu and Li. (2019).
Surface thermal related index	Albedo	Extracted from finer resolution optical visible and NIR band images.	Dominguez et al. (2011); Jiang et al. (2015); Yang et al. (2019).
	Emissivity	Converted and mapped from LULC type map that is created with supervised classifier and high resolution optical imagery.	Inamdar and French (2009); Jiang et al. (2015); Mitraka et al. (2015); Agathangelidis and Cartalis, 2019.
Terrain surface index	Digital elevation model	Elevation values extracted from DEM model at a better than 30 m resolution.	Sismanidis et al. (2015); Jiang et al. (2015); Hutengs and Vohland (2016); Wu and Li. (2019).
	Slope	Slope values extracted from DEM model at a better than 30 m resolution.	Guo et al. (2014); Li et al. (2019); Wu and Li. (2019).
	Aspect	Aspect values extracted from DEM model at a better than 30 m resolution.	Sismanidis et al. (2015); Li et al. (2019); Wu and Li. (2019).
	Solar incident angle	Extracted from DEM data at a better than 30 m resolution and with the same coarse TIR imaging acqusition time in a year.	Li et al. (2018); Hutengs and Vohland (2016).

Table 4
A summary of spectral indices (SIs) frequently used as scaling factors in DLST processes.

Index	Functions and characteristics	Formula	References
AVI	Anomaly Vegetation Index, denoting variation of NDVI in an area.	$NDVI - \overline{NDVI}$	Wu et al. (2019).
BSI	Bare Soil Index, reflecting variation of soil moisture.	$(B3 + B6 - B4 - B1)/(B3 + B6 + B4 + B1)$	Wu et al. (2019b).
DVI	Difference Vegetation Index, reflecting differences of biomass & vegetation cover.	$B4 - B3$	Wu et al. (2019).
EVI	Enhanced Vegetation Index, compared to NDVI, EVI improving sensitivity to high biomass regions and vegetation monitoring.	$2.5(B4 - B3)/(B4 + 6B3 - 7.5B1 + 1)$	Bala et al. (2020).
IBI	Improved New Building Index, see NDBI.	$\left(NDBI - \frac{SAVI+MNDWI}{2}\right) / \left(NDBI + \frac{SAVI+MNDWI}{2}\right)$	Xu (2008).
IVI	Improved New Vegetation Index, characterizing soil, vegetation and impervious surface.	$\left(SAVI - \frac{NDBI+MNDWI}{2}\right) / \left(SAVI + \frac{NDBI+MNDWI}{2}\right)$	Liu et al., 2012; Wu et al., 2019b.
MNDWI	Modified NDWI, high linearly related to LST.	$(B2 - B5)/(B2 + B5)$	Xu (2008).
MSAVI	Modified Soil-Adjusted Vegetation Index, see SAVI.	$\left[2B4 + 1 - \sqrt{(2B4 + 1)2 - 8(B4 - B3)}\right]/2$	Wu et al. (2019).
NDBI	Normalized Difference Built-up Index, high correlation with impervious surface area and less sensitive to seasonal change.	$(B5 - B4)/(B5 + B4)$	Zha et al., 2003; He et al., 2010.
NDMI	Normalized Difference Moisture Index, stronger linearly related to LST, sensitive to vegetation/soil moisture	$(B4 - B5)/(B4 + B5)$	Qian and Cui, 2008; Lillo-Saavedra et al., 2018.
NDVI	Normalized Difference Vegetation index, well-documented Inverse relationship between LST and NDVI and positive relationship between NDVI and soil moisture	$(B4 - B3)/(B4 + B3)$	Rouse et al., 1973; Fassnacht et al., 1997.
NDWI	Normalized Difference Water Index, high linear correlation with LST.	$(B2 - B4)/(B2 + B4)$	McFeeters, 1996; Guo et al., 2017; Bala et al., 2020.
NMDI	Normalized Multi-band Drought Index, monitor the water content of soil and vegetation by using absorption properties in NIR band and absorption differences between NIR and SWIR bands	$[B4 - (B5 - B6)]/[B4 + (B5 - B6)]$	Wang and Qu, 2007; Yang et al., 2011.
RVI	Ratio Vegetation Index, considering the inverse relationship between chlorophyll absorption of red band and high reflectance of NIR band for healthy plant canopies	$B3/B4$	Wu et al. (2019).
SAVI	Soil-Adjusted Vegetation Index, characterizing interaction of soil properties and vegetation systems	$(B4 - B3)(1 + L)/(B4 + B3 + L)$ Where,L = 0.5	Huete 1988; van Leeuwen and Huete, 1996.

Note: 1–6 in $B_{1\text{-}6}$ represent blue, green, red, NIR, SWIR1 (1.6 μm), and SWIR2 (2.2 μm) bands in order.

data. By using ASTER optical data SIs and other SFs, Jeganathan et al. (2011), Chen et al. (2014b), and Pereira et al. (2018) also used ASTER LST data first to upscale to lower resolution LSTs and then to downscale to finer resolution LSTs.

Another commonly used type of SFs for the kernel-based DLST processes includes fraction of vegetation cover (F_{vc}), fraction or abundance images of endmembers, and LULC map, which are all extracted from high resolution optical sensors' data. A vegetation canopy cover or a fraction of vegetation cover (F_{vc}) within a pixel area in percentage (%) or [0, 1] is commonly used as an important SF for some classic and modern DLST processes. F_{vc} may be calculated via NDVI with different definitions/formulas, such as, $(NDVI - NDVI_{min})/(NDVI_{max} - NDVI_{min})$ (Amazirh et al., 2019) and $1 - ((NDVI_{max} - NDVI)/NDVI_{max} - NDVI_{min}))^{0.625}$ (Agam et al., 2007). Fraction images of endmembers or LULC types can be calculated through a spectral unmixing analysis (either linear spectral mixture or multiple endmember linear spectral mixture or extracted from rule images of LULC classification results created with supervised classifiers (e.g., maximum likelihood classifier and support vector machine, SVM). Per LULC map, it is mostly created from high resolution optical multispectral imagers (satellite or airborne sensor's data). Since all the three subtypes of fraction and LULC maps as SFs have close relationships with LST, there are a lot of studies including them as important SFs for the kernel-based DLST processes. For example, Liu et al. (2018b) and Amazirh et al. (2019) downscaled 1000 m LST data to 60 m and 100 m LSTs by using F_{vc} extracted from Landsat optical 30 m NDVI data. To test the performance of a new DLST method, Liu and Su (2016) first used Landsat TM/ETM + LST to upscale to 960 m and then downscale to 480 m, 240 m 120 m and 60 m LSTs with F_{vc} and other SFs extracted from 30 m resolution Landsat optical data. Gustafson et al. (2003) and Pu (2021) downscaled 90 m ASTER LST product to finer resolution LSTs with abundance images of LULC types by spectral unmixing analysis and rule images created with supervised SVM classifier. Deng and Wu (2013b) used thermal spectral unmixing model to downscale TM 120 m LST to 30 m LST with fraction images of LULC types extracted from IKONOS image. Yang et al. (2011) and Sismanidis et al. (2016) used LULC map (created from optical high resolution satellite sensors' data) and other SFs to disaggregate coarse resolution LST data to finer resolution LSTs.

The surface thermal related indices may include surface albedo and emissivity, which are often used as SFs. The albedo is often extracted from visible, NIR and SWIR bands of high-resolution multispectral sensor data, such as from Landsat 8 OLI bands 2–7 (in a linear transformation) (Yang et al., 2019). High resolution spectral emissivity can be obtained via assigning its value to each surface cover type by referring to typical emissivities of various common materials over the thermal spectral range 8–14 μm recommended by Lillesand et al. (2008) or other references. Both the surface thermal related indices have been applied as SFs in DLST processes. For instance, Dominguez et al. (2011), Jiang et al. (2015), and Yang et al. (2019) used the albedo as one of SFs, extract from different sources (NASA-ATLAS, MODIS, and Landsat 8), for DLST process. Similarly, Inamdar and French (2009), Mitraka et al. (2015), Chybicki and Łubniewski (2017), and Agathangelidis and Cartalis (2019) utilized the emissivity as one of SFs in their DLST processes.

In the kernel-based DLST processes, researchers also often use DEM data derived ancillary SFs including elevation, slope, aspect and solar incident angle for their DLST processing studies. This is because the DEM derived SFs directly reflect surface thermal energy budget and thus directly or indirectly influence spatial variation of LST in a study area. For example, Keramitsoglou et al. (2013) and Sismanidis et al. (2016) downscaled MSG-SEVIRI LST data (4 km × 5 km) to MODIS-like 1 km resolution LST using SFs composed by two groups of SFs: The static SFs including land cover, slope, aspect, and altitude maps and the dynamic SFs corresponding to emissivity and SIs maps. Guo et al. (2014), Hutengs and Vohland (2016), and Wu and Li (2019) also used terrain surface indices, land cover data and other SFs to downscale lower resolution LSTs (MODIS and Landsat TM and ASTER) to finer resolution LSTs.

3.2.2. Scaling factor selection

The issue of the SF selection seems not to be very crucial compared to the feature/variable selection for other application purposes of remote sensing. This may be that researchers who conduct their DLST processing studies may have elaborately selected what SFs are the most suitable for their DLST process projects based on their available data sets and research objectives. However, per this literature review, there still are many studies on DLST processes that consider the issue of SF selection to determine a final subset selected from all candidate SFs for the DLST processes. The key reasons for the SF selection are generally lowering SF dimensionality, reducing SF data redundancy and collinearity, and improving efficiency of DLST processing. Currently, there may be three main types of SF selection methods commonly adopted by researchers: (1) Random Forest (RF) algorithm, (2) stepwise regression procedure, and (3) Support Vector Machine-Recursive Feature Elimination (SVM-RFE). With the ranked important scores of each candidate SF, calculated with the RF algorithm, an optimal subset of SFs may be selected from all input SFs with a threshold of importance scores. For example, Li et al. (2019) and Yang et al. (2017) used the RF algorithm calculated importance scores of input SFs (SIs, spectral bands, terrain surface variables, etc.) to select an important subset of SFs to efficiently downscale 1000 m MODIS LST data to relatively higher resolution LSTs. Forward stepwise regression procedure may be used to build robust DLST models. In this procedure, SFs are added in a selected subset in an order of one by one when an SF is added, then the subset increases the most significantly explained model variance (R^2). For instance, Bechtel et al. (2012) used the procedure to find an optimal SF subset for their downscaling LST scheme. The SVM-RFE SF selection method is using RFE that is an embedded ranking-based feature selector (Tuia et al., 2009; Zhang et al., 2017), which chooses a fixed number of high-ranking SFs for subsequent analyses. Therefore, the SVM-RFE SF algorithm, like the RF algorithm, may be used to select an optimal subset of SFs based on their high-ranking values for DLST processes. For instance, Ebrahimy and Azadbakht (2019) applied this SF selection method to choose the three similar high-ranked SFs, namely DEM, NDVI, and a red band, for their downscaling MODIS 960 m LST data to 240 m resolution LST.

3.3. DLST methods and algorithms

To obtain finer spatiotemporal resolution LST data through downscaling coarse spatial resolution but high temporal resolution LST data, many DLST investigators have developed and improved different advanced DLST methods and techniques. Generally, there are two categories of DLST methods and techniques: Kernel-driven process methods and fusion-based process methods. Some researchers also consider the combined (hybrid) categories with these two basic categories (e.g., Xia et al., 2019; Yoo et al., 2020). However, if well understanding the two basic categories, the hybrid category of DLST methods should be easy to understand and master. The kernel-driven processes are the most frequently used thermal downscaling methods, such as classic-based, regression-based, machine-learning-based, TIR spectral unmixing-based, etc. (see their detailed reviews below). This category relies on the relationships between the kernels (SFs) and LSTs to obtain high-resolution LSTs by performing a spatial sharpening process or a TIR spectral unmixing process. The kernels or SFs are extracted from high resolution sensors' data and no-remote sensing ancillary data (see section 3.2 above).

The fusion-based methods are based on fusion algorithms rather than on kernels to obtain spatial details from known fine spatial but low temporal resolution LSTs (e.g., Landsat series) and low spatial but high temporal resolution LSTs (e.g., MODIS), which mostly create high resolution spatiotemporal time series LST products (e.g., Landsat-like LST product). Fig. 3 illustrates the flow diagram of the two basic categories of DLST process methods. Table 5 also summarizes the characteristics, advantages/limitations, and references of the five general types of DLST process methods popularly used during the last four decades. In the following subsections, the five types of DLST methods are reviewed.

3.3.1. Classic-based methods

The earliest studies on the thermal spatial sharpening process were done by such as Tom et al. (1985), Inamura (1993) and Nishii et al. (1996), who used SFs extracted from relative high resolution optical images to enhance or improve relatively low resolution TIR band images. However, the typical and popularly used classic-based downscaling LST (DLST) processing methods are thought Disaggregation of Radiometric Temperature (DisTrad) (Kustas et al., 2003) and Temperature Sharpening (TsHARP) (Agam et al., 2007), and the classic-based methods also include their variants (e.g., TsHARP with local variant (Jeganathan et al., 2011)). The classic-based methods use a simple regression relationship between LST and an NDVI (DisTrad) or fraction of vegetation cover (F_{vc}, TsHARP) to spatially sharpen coarse resolution LST to a finer resolution. To improve the DLST accuracy, the algorithms consider the addition of a "residual" based on the LST differences at coarse resolution between the model estimation and the reference values (i.e. the remotely sensed image to be downscaled). The mechanism underlying the DLST processes relies on correlations between LST and vegetated SFs (NDVI and F_{vc}) that are directly related to the general cooling effect by vegetated surfaces due to shading, biomass, higher relative humidity, and evapotranspiration (Mao et al., 2021). Consequently, such classic-based methods for DLST process methods are limited to be applied in vegetated areas, agriculture areas in growing seasons, and thus, theoretically, they are not suitable for dessert or semi-arid dessert areas covered with sparse vegetation and non-vegetation. Since the classic methods are based on the simple (re-

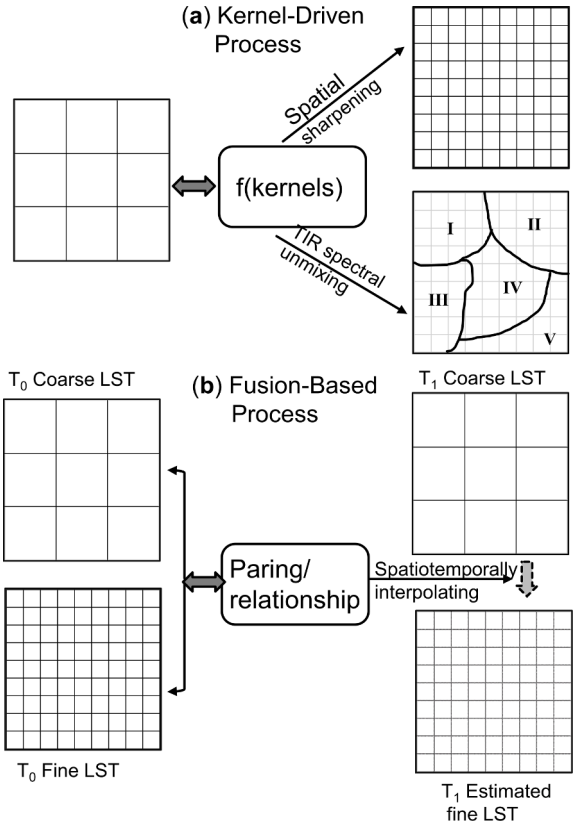

Fig. 3. The flow diagram to illustrate the two basic categories of downscaling LST methods: (a) the kernel-driven process methods and (b) the fusion-based process methods.

gression) relationships between LST and NDVI or F_{vc}, the relationships are site specific. Usually, the classic-based downscaling methods are not only used to create finer resolution LST maps from coarse resolution ones, but also as a standard or testing reference for evaluating the accuracy and performance of newly developed DLST methods.

3.3.2. Regression-based methods

In downscaling LST processes, the regression-based methods are the most popularly used methods with different regression forms and a diversity set of SFs. This type of methods includes linear and non-linear, single SF or multiple SFs regression or polynomial models (e.g., Chen et al., 2012; Gao et al., 2012; Ghosh and Joshi, 2014; Mukherjee et al., 2014; Bonafoni and Tosi, 2017; Gao et al., 2017; Li et al., 2017; Wu and Li, 2019; Wang et al., 2020c; Zawadzka et al., 2020; Pu, 2021). Usually, a regression relationship in different forms of LST with SFs within a study area is empirically determined at a coarse (thermal band) resolution and then applied to a fine (optical band) resolution to generalate a spatial sharpened thermal image. For example, Zawadzka et al. (2020) developed a method that used the Multivariate Adaptive Regression Splines (MARS) models associated with SFs extracted from very high resolution (VHR) hyperspectral aerial imagery and topographic maps to downscale the 100 m Landsat 8 TIRS data to 2–4 m resolutions. Their analysis results indicate that the MARS models could be used to create high resolution LST maps for studying urban thermal environments. Wu and Li (2019) established a nonlinear relationship of LST with input SFs by using a random forest regression model with multitype predictor variables (MTVRF) to downscale LST under various surface characteristics. The MTVRF model produced satisfied results. Maeda (2014) applied simple and multiple regressions to quantify relationships between LST and SFs (e.g., altitude, land covers and NDVI, etc.) in order to downscale 1 km resolution LST to 250 m resolution. By considering geospatial and temporal effects on DLST results, Luo et al. (2021) utilized a geographically and temporally weighted autoregressive (GTWAR) model to disaggregate MODIS 1 km LST to 100 m resolution LST. Compared to the TsHARP, the geographically weighted regression (GWR) (Duan and Li, 2016), the geographically weighted autoregressive (GWAR) and the geographically and temporally weighted regression (GTWR) downscaling LST methods, the GTWAR model provides better performance. Pereira et al. (2018) also used GWR but coupled with area-to-point kriging of regressed residuals to improve the DLST accuracy.

This type of methods is relatively easy to perform, and usually their DLST results are satisfactorily accurate. However, the main limitations of this type are that regression correlations between LST and SFs might be insufficient for some regions (Wu and Li, 2019) and site specific significantly (Mukherjee et al., 2014).

Table 5
A list of method frequently used in DLST and described in detail in subsections 3.3.1 to 3.3.5. The table reports their main characteristics, advantages and limitation, main achievement and some typical references.

The type of DLST methods	Characteristic & description	Advantage & limitation	Main achievements	Typical reference
Classic-based	Simple regression relationship between LST and an NDVI (DisTrad) or fraction of vegetation cover (Fvc, TsHARP) to spatially sharpen coarse resolution LST to finer resolution.	DLST process is simple and running fast; but not suitable for areas with sparse vegetation and no-vegetated areas; the relationships are site specific.	Determination of close relationships between LST and NDVI or Fvc.	Kustas et al., 2003; Agam et al., 2007; Mukherjee et al., 2014.
Regression-based	Regression relationships between LST and SFs (kernels) at a coarse (thermal band) resolution and then applied to the finer resolutions to produce sharpened LSTs.	Relatively easy to perform, and DLST results are satisfactorily accurate. But regression correlations between LST and SFs might be insufficient for some regions and significantly site specific.	Extraction and selection number of effective SFs and choice of an appropriate regression model.	Maeda, 2014; Mukherjee et al., 2014; Luo et al., 2021.
Machine learning-based	Nonlinear relationships between LST and SFs. They usually perform better compared to the regression-based methods and result in higher accuracies of DLST results.	Nondeterministic reasoning, self-learning, self-organization, and excellent nonlinear approximation ability of ANN; insensitivity to multicollinearity of independent variables of RF. But intensive computational resources, complex structure of algorithms, and a black box model, etc.	Determination of representative training samples and structure parameters and selection of key SFs.	Yang et al., 2011; Ghosh and Joshi, 2014; Ebrahimy and Azadbakht, 2019.
TIR spectral unmixing-based	Thermal component (TC) temperatures or radiances by solving the thermal spectral unmixing (TSU) model from coarse resolution data. TC temperature can then be aggregated into different high resolution DLST maps.	TC temperature or radiance instead of component fractions and emissivities can be directly obtained from coarse TIR data, less time consuming even with a large downscaling factor of 30, and higher downscaling accuracy.	Definition and determination of typical thermal components from high resolution optical sensors' data	Mitraka et al., 2015; Wang et al., 2020; Pu and Bonafoni, 2021.
Spatiotemporal fusion-based	Firstly, relationships at an initial time between fine resolution image LST (e.g., Landsat LST) and coarse resolution image LST (e.g., MODIS LST), then downscaling at a target time of coarse resolution LST image to fine resolution LST (fine resolution target time not available)	High spatiotemporal fine resolution (e.g., Landsat-like) LSTs. The effect of mixed pixels and uncertainty for the type of fusion-based methods need to be assessed.	Determination of ideal pair of coarse-/fine- resolution sensors' data at appropriate time points; modelling o spatial and temporal variations of LSTs between two time points.	Gao et al., 2006; Zhu et al., 2010; Xia et al., 2019.

3.3.3. Machine learning (ML)-based methods

During the last decade, machine learning (ML)-based methods have been used to establish no-linear relationships between LST and SFs to downscale coarse resolution LSTs to finer resolutions. The ML-based methods may consist of various artificial neural networks (ANN), support vector machines (SVM), random forest (RF) models, and partial least square model, etc. (e.g., Yang et al., 2011; Ghosh and Joshi, 2014; Hutengs and Vohland, 2016; Bartkowiak et al., 2019; Ebrahimy and Azadbakht, 2019; Xia et al., 2019; Pu, 2021; Xu et al., 2021). The ML-based methods may also include some novel deep learning methods, such as convolutional neural networks, CNN) and recurrent neural networks (e.g., Yin et al., 2021). They usually perform better compared to the regression-based methods. The higher accuracy can be ascribed to the fitting of nonlinear relationships between LST and SFs (Li et al., 2019) leading to a more reliable approximation of these relationships (Mao et al., 2021). For example, Yang et al. (2011) used ANN models trained with the 990 m resolution MODIS LST product and the corresponding input SFs (i.e., area ratios and endmember indices) to estimate the 90 m resolution DLST. The DLST was verified with ASTER LST product and was basically consistent with the latter. To address the issue of nonlinearity and spatial nonstationarity in DLST processes, Xu et al. (2021) proposed a multi-factor geographically weighted machine learning (MFGWML) method to downscale the 30 m LST data retrieved from Landsat 8 images to 10 m LST data mainly based on Sentinel-2A images derived SFs. MFGWML used three excellent machine learning algorithms (namely extreme gradient boosting, multivariate adaptive regression splines, and Bayesian ridge regression) and a geographically weighted regression algorithm to fit nonlinear relationships and allow for spatial nonstationarity. Their results indicate that MFGWML could characterize the local heterogeneity and obtain reliable and accurate DLST results. Ghosh and Joshi (2014) conducted a set of experiments to downscale LST retrieved from Landsat ETM + thermal image with SFs extracted from EO1-Hyperion hyperspectral data over three different geographic locations with different landscape characteristics. They selected a partial least square regression and two machine learning algorithms, namely boosting machine (GBM) and SVM, for processing DLST. Compared to the DLSTs produced by DisTrad sharpening model and the regression model, GBM and SVM have created much better DLST results. To disaggregate MODIS ~1 km LST product to ~250 m resolution, Hutengs and Vohland (2016) used a random forest (RF) regression approach with SFs of terrain features, land cover data, and surface reflectances. Hutengs and Vohland (2016) found that the RF model improved the DLST accuracy up to 19% with respect to the commonly used TsHARP sharpening method. With MODIS 1000 m LST and Landsat LST data sets, Yin et al. (2021) developed a deep learning-based spatiotemporal temperature fusion network (STTFN) based on CNNs handling the non-linearity of LST temporal changes for creating finer spatiotemporal resolution LST products. Their experimental results demonstrate the better performance of the STTFN algorithm than other spatiotemporal-based methods (see detailed review in section 3.3.5 below).

There are many advantages with different ML methods, including nondeterministic reasoning with a complex causality due to its self-learning/-organization, error tolerance, and excellent nonlinear approximation ability of ANN; rapid processing ability of high-dimensional data with SVM; and insensitivity to multicollinearity of independent variables to RF (Li et al., 2019). However, the major limitations for the ML technique-based methods may include intensive computational resources, complex structure of algorithms, and a black box model, etc.

3.3.4. TIR spectral unmixing (TSU)-based methods

Compared to the spatial sharpening kernel-driven methods above (i.e., classic-, regression-, and ML-based DLST methods), there are fewer studies on DSLT processes based on thermal spectral unmixing (TSU). The earlier TSU-based DLST methods could be back to early 1980s when Dozier (1981) and Matson and Dozier (1981) published their initial explored works based on thermal spectral unmixing principle with moderate optical multispectral imagery. More recently, the TSU-based DLST methods can be described as follows: thermal component (TC) temperatures within a pixel area are decomposed based on multi-temporal, -spatial, -spectral, and/or -angular observations (Zhan et al., 2013). The TC temperatures or radiances at an initial high resolution, created by solving the TSU model from coarse resolution thermal (or LST) data, can then be used to produce different high resolution DLST maps (Deng and Wu, 2013b, 2013a; Ma et al., 2016; Zhu et al., 2018; Wang et al., 2020; Pu and Bonafoni, 2021). For example, Deng and Wu (2013b) proposed a VHR spectral unmixing and thermal mixing (VHR-SUTM) approach to disaggregate LST to a high resolution. The VHR-SUTM method may include: (1) spectral unmixing with IKONOS data to obtain fractions of land cover types that respond to unique thermal characteristics, and (2) thermal unmixing with lower resolution Landsat TM LST and corresponding land cover fractions to estimate high resolution LST pixel values. Their thermal spectral unmixed results indicate that the estimated LST map was high consistent with the corresponding resolution of retrieved LSTs. Li et al. (2021) also developed a TSU-based method, named temperature downscale with data Fusion and spectral unmixing, to unmix Landsat 8100 m LST to 16 m high resolution LST with surface features abundances extracted from Gaofen-1 data. The results indicate that the TSU model can effectively estimate high resolution LST and reflect the spatial variation of the LST. Mitraka et al. (2015) developed a TSU-based method for downscaling low-resolution MODIS TIR data using SFs extracted from optical Landsat sensors to obtain time-series high spatial resolution LSTs. The results indicate that the proposed approach shows a high potential of being operationally used in the near future to produce high spatiotemporal resolution LSTs in cities. With VHR airborne LST and hyperspectral optical data (1.25 m resolution), Liu et al. (2016) first upscaled both LST and optical data to 4 m, 8 m, 16 m and 32 m resolution, then used a TSU model to downscale to 16 m, 8 m, 4 m resolution LSTs. The analysis results show a well agreement between the DLST and the reference LST by using both visual interpretation and quantitative accuracy metrics.

With the TSU-based methods, one advantage is that high resolution thermal component (TC) temperature or radiance can be directly created from coarse TIR data (LST or radiance). For instance, Wang et al. (2020) proposed the TC-based spectral unmixing technique to create TC radiance. The TSU technique may be used directly to solve a system of linear spectral mixture models encoding the TC-LST (or thermal radiance) relationship at a coarse resolution (e.g., MODIS 1000 m LST), and then the solution is applied to a fine resolution to obtain fine resolution LST results. Their results indicate that downscaled LST could differentiate temperatures over major land types and capture both seasonal and diurnal LST dynamics. Pu and Bonafoni (2021, 2022) modified the TSU model developed by Wang et al. (2020) for directly downscaling the ASTER LST data to high and very high resolution LSTs. Their analysis results indicate that the modified TSU model for unmixing TC temperatures at an initial high resolution was effective and advanced in DLST processing compared with their previous works and those in current literature. In general, this type of DLST methods is less time consuming even with a large downscaling factor of 30 (Wang et al., 2020) and outperformed classic downscaling techniques significantly.

3.3.5. Spatiotemporal fusion-based methods

As conceptually illustrated by Fig. 3b, spatiotemporal fusion-based methods first construct relationships at an initial time between fine resolution (usually low temporal resolution) image LST (e.g., Landsat LST) and coarse resolution (usually high temporal resolution) image LST (e.g., MODIS LST), then downscale a target time coarse resolution image LST to fine resolution LST when the target time fine resolution LST is not available (Yoo et al., 2020). During the last two decades, the spatiotemporal fusion-based methods can be classified into two general types: (1) the methods based on the spatial and temporal adaptive reflectance fusion models (STARFM) and (2) the methods based on unmixing theory (Yang et al., 2020). The first type of methods assumes that the ratio of coarse pixel value to neighboring similar pixels does not change over time, while the second type assumes that the value of each coarse resolution pixel is a linear combination of the responses of all endmembers within the coarse pixel. The two types of methods all use spatial relationships between coarse/native- and fine/target-resolution images acquired from different sensors, and the temporal variation between the initial and target times to interpolate/predict fine-resolution image LST at the target time. The spatial resolution of the interpolated LST image corresponds to that of the fine-resolution image (e.g., 100 m LST Landsat TIRS data) while the temporal resolution of the interpolated LST image corresponds to that of the target time coarse resolution (e.g., daily MODIS LST data) (Xia et al., 2019). In short, the resultant fused LST data with the type of methods possess high spatiotemporal resolution characteristics of LSTs originally coming from fine spatial resolution sensors (e.g., Landsat TIRS) and high frequency sensors (e.g., MODIS).

Per the 1st type of the methods, the most popularly used method for DLST processing is the STARFM, which originally fuses the daily MODIS and the 16-day Landsat surface reflectance data to produce a synthetic daily surface reflectance Landsat-like data (Gao et al., 2006). Later, the method was directly used to produced high temporal resolution and fine spatial resolution LST products. For example, Liu et al. (2018b) used the STARFM method to downscale MODIS 1000 m LST to produce LST data at a fine resolution of 60 m and a fine temporal resolution of 1 day with Landsat TM data. More similar application works with the STARFM may also include those by Wu et al. (2015) and Liu and Weng (2018) etc. Since the STARFM might not be sensitive to heterogeneous landscapes,

many researchers have improved the method, such as the enhanced STARFM (ESTARFM) (Zhu et al., 2010) and FSDAF (flexible spatiotemporal data fusion) (Zhu et al., 2016). The ESTARFM can increase the data fusion accuracy by considering heterogeneous landscapes, while FSDAF can not only consider heterogeneous landscapes but also maintain spatial details within a study area (Zhai et al., 2020). The unmixing-based spatiotemporal models, estimating high-resolution LST data based on a linear spectral mixing model, may include ISTBDF (improved spatiotemporal Bayesian data fusion) (Xue et al., 2019), ISTRUM (improved spatial and temporal reflectance unmixing model), and STDAF (spatial temporal data fusion approach) (Wu et al., 2012). For instance, Ma et al. (2016) downscaled coarse resolution MODIS LST data to create synthesize time series of Landsat-like products by using the ISTRUM. This type of methods can predict an accurate estimation of LST by grouping similar pixels and calculating their average LST.

Different from kernel-driven methods, the spatial detailed information with this type of fusion-based methods is obtained from known fine resolution LST data rather than kernels. To further improve the prediction accuracy created with the spatiotemporal fusion-based methods, many researchers also made an effort on combining advantages of both kernel-driven and fusion-based process methods (i.e., detailed spatial information with a kernel-based method and high frequency time series LST products with fusion-based method (Yoo et al., 2020)). One type of spatiotemporal fusion-based methods considers the synergy of the kernel-driven and fusion-based approaches to produce time series high spatiotemporal Landsat-like LST products. For example, Xia et al. (2018) proposed two strategies for combining regression-based method and fusion-based methods to create high spatiotemporal resolution LST product, namely, the “regression-then-fusion” (R–F) and “fusion-then-regression” (F-R) methods. After testing Landsat 8 and ASTER data (first upscaling to coarse resolution then using R–F and F-R strategies to downscale to Landsat-like and ASTER-like LST products), their results clearly indicate that the R–F strategy performed better than the F-R strategy when the regression error at the start time was smaller than that at the target time, and otherwise, the F-R strategy was better than the R–F one. Xia et al. (2019) proposed a weighted combination of kernel-driven and fusion-based methods (CKFM) to further improve the spatiotemporal resolutions of time series LSTs. The CKFM is more accurate and robust compared to the kernel-driven method with an improvement of 0.1–0.6 K, and it may reconstruct more spatial details than those by a fusion-based method when it was used to downscale daily MODIS 1 km LSTs to 30 m resolution LSTs with Landsat 8 data.

By this literature review on applications of this type of methods, most investigations were found on producing high spatiotemporal resolution synthetic LST products (e.g., Landsat-like LST data series) by mostly fusing MODIS – Landsat data. More advanced spatiotemporal fusion-based methods include synergic methods (e.g., Xia et al., 2019) by combining the kernel-driven process with the fusion-based process methods, which more emphasize on how to efficiently deal with spatial heterogeneity of landscapes (spatial variation of LST) and time change (temporal variation of LST) between any two time points. This is a key point or a research direction. In addition, it is necessary that the effect of mixed pixels with different LULC cover types on the high spatiotemporal LSTs and uncertainty for the type fusion-based methods need to be assessed by considering the optical/thermal sensors’ noises, LST retrieval errors, and spatial/temporal variations of LST induced by heterogenous landscapes, mixed pixels, and seasonal change (Mao et al., 2021).

3.4. DLST statistics-based models vs physical-based models

DLST methods listed in Table 5 and detailed in this section (classic-based, regression-based, machine learning-based, TIR spectral unmixing-based, spatiotemporal fusion-based) are mainly based on statistical approaches leading to empirical relationships. A limitation of these approaches, although they can provide good performance, is the lack of a clear physical mechanism in the downscaling modelling, resulting in difficult understanding of the interactions between scaling factors and LST. Furthermore, these empirical regressive relationships hinder the extension of a statistical LST downscaling method to other study areas.

For instance, LST downscaling methods can also be divided in physical mechanism-based models (Dozier, 1981; Nichol, 2009; Guo and Moore, 1998; Liu and Pu, 2008, Liu and Zhu, 2012) and statistics-based models. Physical DLST methods establish meaningful relationships by considering the physical mechanism of a mixture pixel and the thermal radiation theory. For example, Nichol (2009) proposed the emissivity modulation model to improve the spatial resolution of thermal radiation. Guo and Moore (1998) proposed the pixel block intensity modulation (PBIM) to integrate the topographic spatial details at finer resolution into the thermal images. Liu and Pu (2008) developed a new physical model based on spectral mixture analyses, enhanced by Liu and Zhu (2012).

Although physical-based methods facilitate the scientific interpretation of the results, the implementation complexity can limit their application. Compared with physical models, statistics-based models are generally easier to implement and have become more popular.

4. Spatial scaling effect in downscaling LST processes

Many DLST investigations have proved that a spatial scaling effect does exist in DLST processing, especially DLSTs at VHR resolutions. Per easily understanding DLST results, we can define the spatial scaling effect as an error in the downscaled LST process at a target (high) resolution, which may be understood as a difference between DLST and true/reference LST at high resolutions (Chen et al., 2012; Zhou et al., 2016; Pu and Bonafoni, 2021). In this section, the causes producing the spatial scaling effect in DLST processes are reviewed and discussed, along with methods/techniques for reducing it.

4.1. Spatial scaling effect

Based on the literature review, the spatial scaling effect in DLST processes is mainly caused by a basic assumption in DLST processes, which assumes that the LST– descriptors relationship (linear or non-linear) at a native (coarse) resolution is scale-invariant at different DLSTs at finer resolutions (Kustas et al., 2003; Agam et al., 2007). The assumption is mostly problematic in real DLST processing cases due to spatial variation changes of the spatial resolution and spatial extent in heterogenous environments (Chen et al.,

2012; Ghosh and Joshi, 2014; Zhou et al., 2016). The variation of spatial resolution can be caused by the change of the pixel size that is associated with the change of spatial variation within a specific pixel area, while the variation of spatial extent can be related to different heterogeneous landscapes at a large scale within a scene of imagery. The former (spatial variation) may be directly or indirectly related to the spatial variation of bio- and physical surface materials (e.g., greenness patch size and bare soil patch size variations) within the different pixel size areas while the latter is due to existing different landscapes (e.g., with different LULC types: agriculture, grassland, urban land use) in a study area. Both variations in a scene of imagery directly result in the spatial scaling effects in DLST processes.

There are many studies that have demonstrated the spatial scaling effects in DLST processes caused by either or both the spatial variations discussed above. For example, Chen et al. (2012) studied the scaling effects of variation of spatial resolution and spatial extent on DLST results by using relationships between vegetation index and LST at/within different resolutions and extents, based on two scenes of ASTER data separately covering grassland and cropland. They found that the relationships between vegetation index and LST at different spatial resolutions were very different within different spatial extents. Zhou et al. (2016) directly proved that the scale effect was closely associated with the varying spatial distribution of the LST and corresponding SFs at the coarse and target resolutions. They utilized different linear regression models that were developed for different target resolutions to evaluate the spatial scale effect in DLST processes from moderate resolution sensors (e.g., ASTER TIR data and Landsat 8 TIRS data) to higher resolutions. Their results indicate that the scale effect depended on the variations of SFs, the phenology, and both of native and target resolutions. There are many other investigations proved the scaling effect caused by the variations of both spatial resolution and spatial extent, including Jeganathan et al. (2011) who analyzed the scaling effect through DLSTs from 1 km MODIS LST product downscaled to 810 m, 630 m, …, and 180 m resolution LSTs and indicated the scaling effect caused by different spatial resolutions and Ghosh and Joshi (2014) who also confirmed that the scale effect is induced by a spatial variation of the surface characteristics.

4.2. Assessing and reducing scaling effect

As reviewed above, although advanced statistical models and machine learning methods have improved DLST results at finer resolutions via reducing error (spatial effect) between downscaled LSTs and their reference LSTs, the spatial scaling effect still exists on DLST results at finer resolutions. Many researchers have made efforts to quantify the scaling effect in DLST processes by using different measurements and approaches. For example, Chen et al. (2012) used the slope of relationships of VI – LST at different spatial resolutions and within different spatial extents to quantify the scaling effect, while Zhou et al. (2016) also utilized the slope change regression models at different target resolutions and a native resolution. Jeganathan et al. (2011) confirmed both slope and intercept in linear regression models depending on native and target resolutions. There were more approaches used to measure the scaling effect, including an error estimation method by Chen et al. (2014), who used an equivalent random sample size and a semivariogram approach by Pu (2021) that when lag distances of spatial resolutions or spatial extents are longer than the range in a semivariogram, the scaling effect may be ignored, but, when the lag distance is shorter than the range of the semivariogram, the effect is statistically significant.

Given the fact that the spatial scaling effect always exists on DLST results despite the advancement of DLST methods, how to develop some methods and techniques that can be used to directly reduce the scaling effect on DLST maps is definitely significant in improving DLST results. However, only one initial effort in the literature was found to try to directly reduce the scaling effect. Pu and Bonafoni (2021) developed a new approach with a correction term (CT) expression that was used to correct the scaling effect on the basis of an analysis of the degree of heterogeneity of surface features/materials within a pixel area at a specific resolution. This CT was derived and added to the DLST maps after the residuals were already added. Their experimental results indicate that the new approach was effective in improving DLST maps (up to 30%) by reducing the scaling effect at VHR resolutions.

In the above description, it is assumed that most of the spatial scaling effect in downscaling results is mainly caused by the assumption that the relationships between LSTs and surface descriptors (scale factors or kernels) are scale invariant. It is worth to mentioning that the original data also present spatial scale effects, such as the differences between fine resolution NDVI and coarse resolution NDVI. Therefore, a further approach to reduce the scale effects in DLST can be based on the intercalibration of the descriptors and LST between different satellite sensors at different resolution, for example MODIS and Landsat sensors (Bindhu et al., 2013).

A further influencing factor on the scale effects in downscaling LST processes is the moving-window setting. Previous studies addressed this issue impacting the accuracy of DLST at different scales (Jeganathan et al., 2011; Zakšek and Oštir, 2012; Garrigues et al., 2006; Gao et al., 2017). The performance of a moving window setting is dependent on the extent of surface heterogeneity (Li et al., 2022). For mixed surfaces, a localized window performed better than the global window. For almost homogeneous surfaces, the global window performed better than a localized window.

5. Limitations and future research directions

5.1. Existing limitations and constraints

Many factors determine and influence the success and accuracy of DLST processes. The factors may be considered: a) reliability and accuracy of various scaling factors (SFs) determined and extracted from high resolution remote sensing and non-remote sensing data, b) scale factor between coarse and finer resolution, c) spatial extent, d) generalization of DLST models/algorithms, and e) spatial scaling effect issue. Literature review indicates that existing methods/techniques used for accurate DLST processes under certain environmental settings and backgrounds frequently suffer from some limitations and/or constraints.

There always exists an uncertainty of DLSTs despite how advanced of a kernel-driven or fusion-based process DLST model and algorithm applied. Such an uncertainty of DLST can be associated with a) potential errors in determining, extracting and selecting SFs

(Yang et al., 2011), b) errors caused by using a general global scaled model of DLST due to spatial variation changes of spatial resolution and spatial extent (Chen et al., 2012; Gao et al., 2017), and c) errors caused by nonlinearity of temporal change of LST with SFs. To improve efficiency of DLST processing, as discussed in section 3.2, there are many types and characteristics of SFs that can be adopted in DLST processes, in which the potential errors may directly influence the accuracy (uncertainty) of a relationship of LST with SFs at a native (coarse) resolution. For example, Bechtel et al. (2012) used the stepwise procedure to find an optimal SF subset for their downscaling LST scheme, while Tuia et al. (2009) and Zhang et al. (2017) utilized SVM-recursive feature elimination approach to choose an ideal subset of SFs based on their high-ranking values for their DLST processes. Based on this literature review, most existing kernel-driven DLST models are at a general global scale, which may suffer variations of spatial resolution and spatial extent and thus lead to a higher uncertainty of DLSTs (Chen et al., 2012). To optimize DLST accuracy and computational complexity, Gao et al. (2017) adopted an optimal moving-window size as a local window strategy for DLST processing and demonstrated the better performance of the local window approach over a global window one. Currently, most fusion-based models (e.g., STARFM and ESTARFM) assume that the DLST output with high spatiotemporal resolution (e.g., Landsat-like LST product) is linearly related to their input LSTs. Although surface cover types and landscape components do not change significantly within a certain time period, reflectance may change slowly over time (e.g., physical parameter change), which may result in corresponding LST quick temporal change in a nonlinear way (Mohamadi et al., 2019). To solve the problem, fusion-based models need considering a nonlinear LST temporal change to improve the quality of output DLSTs (e.g., the SADFAT may consider using the MODIS annual cycle parameters, discussed by Weng et al. (2014)).

Existing literature review indicates that most DLST models/techniques lack generalization and most DLST studies are study site specific and thus difficult or impossible to extend them to outside of a study area. Currently, exploring and assessing new methods/techniques for downscaling DLST is mostly conducted in a relatively small test site (area). It is worthy of noting that only a few of efforts among those studies reviewed in this paper have used more than one study area for DLST processing (e.g., Liu et al., 2019; Peng et al., 2019; Wu et al., 2019; Wang et al., 2020; Pu and Bonafoni, 2021; Yin et al., 2021). The performance of the methods/techniques often varied by the characteristics of bio-physical conditions and environmental settings. For example, the methods using VIs, NDVI or EVI, as SFs (for DisTrad and TsHARP) might not work properly for areas with less or no vegetation cover (Mukherjee et al., 2014; Qiu et al., 2018). Any developed DLST models/methods and findings derived from such a single and small test site may be unreliable and already biased. Two reasons can explain it: (1) a single or small test site cannot fully reflect and account for the spatial variations of bio-physical conditions and environmental settings that a newly developed method/algorithm needs to account for; (2) the collected thermal and optical data from such a single small test site may be biased (due to a relatively narrow range of temperature and reflectance variation of surface cover types/materials) towards some favorable conditions. To ensure the generalized capability of DLST methods, one possible solution is to assess them over multiple areas/sites with different conditions and data sets and optimize the related parameters (Yoo et al., 2020).

After a relatively extensive literature review and compared with some traditional DLST methods, many advanced methods and techniques (e.g., machine learning methods) provide an improvement of the accuracy of DLST maps to a certain extent (Chen et al., 2012; Pu, 2021). However, as discussed in section 4, a certain spatial scaling effect still exists in DLST processes, especially at high resolutions. Therefore, it is important to develop a new approach to directly correct or compensate the spatial effect on DLST maps at finer resolutions.

Lastly, a further limitation is the lack of a unified evaluation method for DLST results accuracy, that would simplify the comparison of the performance of different approaches.

5.2. Future research directions

According to this paper review of TIR remote sensing data downscaling published during the last four decades, the future research directions of thermal downscaling may be drawn as follows: a) further reducing the uncertainty of DLST results, b) developing novel DLST models and algorithms and d) directly reducing the spatial scaling effect in DLST processes.

The first general general direction is the development of some methods and techniques reducing the uncertainty of DLST results by considering optimal subset of SFs, establishing DLST model with a localizing moving window strategy and adopting a nonlinear model of temporal change for a fusion-based model. Currently, a few of studies have tested some novel methods and techniques and demonstrated that using a comprehensive and optimal subset of SFs (e.g., Tuia et al., 2009; Zhang et al., 2017), a localizing moving window strategy (Zhan et al., 2012; Gao et al., 2017; Peng et al., 2019), and developing a fusion-based model with nonlinearity of temporal change (e.g., Weng et al., 2014 for SADFAT model) can result in significant improvement of DLST results. However, more efforts still need to be made in the future in developing such novel methods and techniques in downscaling coarse spatial LST to finer resolution LSTs.

More specific future research directions may focus on developing or refining existing advanced models and methods, such as deep learning, local and temporal weighted autoregressive regression (GTWAR) and a weighted combination of kernel-driven and fusion-based methods (termed CKFM) to enhance the spatiotemporal resolutions of time series LSTs. As reviewed in section 3.3, while most researchers developed and used various statistical models for coarse resolution LST downscaling, a few of them have utilized advanced machine learning methods. For example, a CNN model has been used in LST downscaling in an image fusion-based method by Yin et al. (2021), and a more advanced deep-learning model (i.e., generative adversarial network (GAN)) could improve the image pan-sharpening performance than the CNN (Liu et al., 2018c; Zhang et al., 2021). Luo et al. (2021) proposed the GTWAR approach to downscale the 1 km MODIS LST to 100 m. In this model, they considered the temporality, spatial heterogeneity, and spatial autocorrelation of the LST and SF data simultaneously. The GTWAR downscaling model could facilitate improvements in downscaling LST in time series. To further improve high spatiotemporal Landsat (or other fine spatial resolution)-like LST time series products by using

spatiotemporal fusion-based method, Xia et al. (2019) proposed the CKFM model to enhance the spatiotemporal resolutions of time series LSTs by compensating the limitations kernel-driven process and fusion-based process methods separately in DLST processes. The kernel-driven process can offer spatial details from high resolution optical images, while the fusion-based process can create spatiotemporal information. Their testing results indicate that the CKFM is more accurate and robust than other kernel-driven or fusion-based methods and it can reconstruct more spatial details for various environmental studies.

Those advanced and novel methods and techniques have demonstrated their excellent performance and robustness. However, more efforts still need. For example, for the machine learning methods, their performances could be further enhanced if additional input data such as in-situ LST or other numerical model data are used together for a CNN. Per the GTWAR model, the SFs are not comprehensive and optimal and the temporal change too narrow. For the CKFM model, it may be modified with a temperature cycle model (e.g., diurnal/annual temperature cycle models) to further improve high spatiotemporal resolution time series LST product. In developing a novel spatiotemporal fusion-based method, how to deal with spatial heterogeneity of landscapes (leading to spatial variation of LST) and temporal change (inducing temporal variation of LST) between any two time points should be a key point or a research direction.

Given that the scaling effect always exists in DLST processes, especially at very high resolutions, how to directly reduce the effect by developing some novel methods should be another direction. The initial effort was made by Pu and Bonafoni (2021, 2022) who justified that the spatial scaling effect on DLST maps is related to the degree of heterogeneity of landscapes associated with spatial changes of surface features/materials within pixels at specific resolutions. This issue was proved early by Garrigues et al. (2006a, 2006b) by quantifying the heterogeneity within a pixel area for mapping NDVI and LAI with moderate resolution remote sensing data and non-linear estimation processes. Garrigues et al. (2008) also employed a geostatistical linear model to assess the landscape spatial heterogeneity with high resolution red and NIR band images. Based on the theory, Pu and Bonafoni (2021) developed a novel method with a correction term expression to directly correct the effect on DLST maps. The analysis results indicate that the new method could significantly reduce the DLST error. The establishment of physical-based models in DLST processes could reduce the spatial scale effects, by implementing a physical relationship at the coarse resolution: this hypothesis should be explored and verified, even if the implementation could be more complex with respect to statistics-based model.

6. Concluding remarks

In this review paper, a total of 223 publications related to the investigations of TIR remote sensing data downscaling were reviewed. An overview on TIR sensors/systems data and existing DLST methods and techniques was conducted, especially for DLST processes with polar and geostationary orbits TIR sensors' data. After conducting the review, concluding remarks and recommendations are summarized as follows.

1). During last four decades, especially after 2000, most investigations on DLST processes used coarse spatial resolution but high temporal resolution MODIS TIR data. This was just a perfect match for the advent of MODIS sensor onboard Terra and Aqua around 2000. MODIS sensor acquires TIR data at 1 km spatial resolution and 1–2 days temporal resolution.
2). Compared to fusion-based method, the kernel-driven methods are the most frequently used. This downscaling category relies on relationships between the kernels (SFs) and LSTs to obtain high-resolution LSTs by performing a spatial sharpening process or a TIR spectral unmixing process. It is relatively easy to perform and can potentially produce spatial details of LST.
3). To enhance LST resolution and increase the accuracy of DLST results with kernel-driven methods, after 2010, the machine-learning (ML) methods have demonstrated their excellent performance and robustness. Usually, such advanced ML methods/algorithms/models can generate higher accuracies of DLST maps compared to those created with other DLST techniques.
4). Most studies on generating high spatiotemporal fused LST data were performed by mostly fusing MODIS – Landsat datasets to create a high temporal resolution Landsat-like LST data series. More advanced spatiotemporal fusion-based methods combine the kernel-driven process with the fusion-based methods. The synergic process can create both spatial details from optical bands and spatiotemporal information.
5). In this review, three limitations or constraints were identified and recommended to overcome in future works. They include (1) an uncertainty of DLST products created despite the advanced DLST algorithm applied; (2) lack of generalization, since most DLST studies are study site specific and thus it is difficult to extend them outside the study area; and (3) a certain spatial scaling effect always exists in DLST processes, especially at high resolutions.
6). The recommended three future research directions are: 1) reducing the uncertainty of DLST results, 2) developing novel DLST models and algorithms and 3) directly reducing the spatial scaling effect in DLST processes. Currently, a few of studies have tested some novel methods and techniques and demonstrated the efficiency in DLST processes by using a comprehensive and optimal subset of SFs, a localizing moving window strategy, and developing the fusion-based model with nonlinearity of temporal change over time. However, more efforts still need to be made in the future in developing such novel methods and techniques. However, more emphasis on how to efficiently deal with spatial heterogeneity of landscapes (spatial variation of LST) and time change (temporal variation of LST) between any two time points is a key point or a research direction. Given the fact that the scaling effect always exists in DLST processes, especially at VHR resolutions, how to directly reduce the effect by developing some novel approaches should be another direction.

Declaration of competing interest

The authors declare that they have no known competing financial interests or personal relationships that could have appeared to influence the work reported in this paper.

Data availability

Data will be made available on request.

Acknowledgements

This work was supported by the University of South Florida, USA.

Appendix

Abbreviations and acronyms used in this paper

AATSR	Advanced Along-Track Scanning Radiometer
AGRI	Advanced Geosynchronous Radiation Imager
ATSR	Along-Track Scanning Radiometer
ANN	artificial neural network (model)
ASTER	Advanced Spaceborne Thermal Emission and Reflection Radiometer, sensor
AVHRR	Advanced Very High Resolution Radiometer
CNN	convolutional neural networks
DisTrad	Disaggregation of Radiometric Temperature
Envisat	Environmental Satellite
ERS	European Remote Sensing Satellite
ESTARFM	enhanced spatial and temporal adaptive reflectance fusion model
ETM +	Enhanced Thematic Mapper Plus
FSDAF	Flexible Spatial and Temporal Adaptive Reflectance Fusion Model
GAN	generative adversarial network
GOES	Geostationary Operational Environmental Satellite
INSAT	Indian National SATellite
LSE	Land Surface Emissivity
LST	Land Surface Temperature
LULC	land use/land cover
ML	machine learning
MODIS	MODerate-resolution Imaging Spectroradiometer
MS	multispectral
MSG	Meteosat Second Generation
NDVI	normalized difference vegetation index
NIR	near-infrared
OA	overall accuracy
PCS	PC Spectral Sharpening
RF	random forest
SEVIRI	Spinning Enhanced Visible and Infrared Imager
SF	Scaling factor (kernel)
SLSTR	Sea and Land Surface Temperature Radiometer
STDF	spatiotemporal data fusion
STARFM	spatial and temporal adaptive reflectance fusion model
SWIR	shortwave infrared
SVM	support vector machine
TIR	thermal infrared (3–14 mm)
TM	Thematic Mapper
TsHARP	Temperature Sharpening
UAV	unmanned aerial vehicle
UHI	urban heat island
VHRR	Very High Resolution Radiometer
VIRR	Visible and Infrared Radiometer
VNIR	visible-near infrared (0.4–1.0 mm)

References

Agam, N., Kustas, W.P., Anderson, M.C., Li, F., Neale, C.M.U., 2007. A vegetation index-based technique for spatial sharpening of thermal imagery. Remote Sens. Environ. 107, 545–558.

Agathangelidis, I., Cartalis, C., 2019. Improving the disaggregation of MODIS land surface temperatures in an urban environment: a statistical downscaling approach using high-resolution emissivity. Int. J. Rem. Sens. 40 (13), 5261–5286. https://doi.org/10.1080/01431161.2019.1579386.

Amazirh, A., Merlinb, O., Er-Raki, S., 2019. Including Sentinel-1 radar data to improve the disaggregation of MODIS land surface temperature data. ISPRS J. Photogrammetry Remote Sens. 150, 11–26. https://doi.org/10.1016/j.isprsjprs.2019.02.004.

Anderson, M.C., Allen, R.G., Morse, A., Kustas, W.P., 2012. Use of Landsat thermal imagery in monitoring evapotranspiration and managing water resources. Remote Sens. Environ. 122, 50–65.
Bai, L., Long, D., Yan, L., 2019. Estimation of surface soil moisture with downscaled land surface temperatures using a data fusion approach for heterogeneous agricultural land. Water Resour. Res. 55, 1105–1128. https://doi.org/10.1029/2018WR024162.
Bala, R., Prasad, R., Yadav, V.P., 2020. Thermal sharpening of MODIS land surface temperature using statistical downscaling technique in urban areas. Theor. Appl. Climatol. 141, 935–946. https://doi.org/10.1007/s00704-020-03253-w.
Bartkowiak, P., Castelli, M., Notarnicola, C., 2019. Downscaling land surface temperature from MODIS dataset with random forest approach over alpine vegetated areas. Rem. Sens. 11 (11), 1319.
Bechtel, B., Zakšek, K., Hoshyaripour, G., 2012. Downscaling land surface temperature in an urban area: a case study for Hamburg, Germany. Rem. Sens. 4, 3184–3200. https://doi.org/10.3390/rs4103184.
Bindhu, V.M., Narasimhan, B., Sudheer, P., 2013. Development and verification of a non-linear disaggregation method (NL-DisTrad) to downscale MODIS land surface temperature to the spatial scale of Landsat thermal data to estimate evapotranspiration. Remote Sens. Environ. 135, 118–129.
Bisquert, M., Sánchez, J.M., Caselles, V., 2016. Evaluation of disaggregation methods for downscaling MODIS land surface temperature to Landsat spatial resolution in Barrax test site. IEEE J. Sel. Top. Appl. Earth Obs. Rem. Sens. 9 (4), 1430–1438.
Bonafoni, S., 2016. Downscaling of landsat and MODIS land surface temperature over the heterogeneous urban area of milan. IEEE J. Sel. Top. Appl. Earth Obs. Rem. Sens. 9 (5), 2019–2027. https://doi.org/10.1109/JSTARS.2016.2514367.
Bonafoni, S., Tosi, G., 2017. Downscaling of land surface temperature using airborne high-resolution data: a case study on Aprilia, Italy. Geosci. Rem. Sens. Lett. IEEE 14 (1), 107–111.
Bonafoni, S., Anniballe, R., Gioli, B., Toscano, P., 2016. Downscaling Landsat land surface temperature over the urban area of Florence. Eur. J. Rem. Sens. 49, 553–569. https://doi.org/10.5721/EuJRS20164929.
Chen, X.H., Yamaguchi, Y., Chen, J., Shi, Y.S., 2012. Scale effect of vegetation-index-based spatial sharpening for thermal imagery: a simulation study by ASTER data. Geosci. Rem. Sens. Lett. IEEE 9 (4), 549–553.
Chen, X., Li, W., Chen, J., Rao, Y., Yamaguchi, Y., 2014. A combination of TsHARP and thin plate spline interpolation for spatial sharpening of thermal imagery. Rem. Sens. 6, 2845–2863. https://doi.org/10.3390/rs6042845.
Chen, X., Li, W., Chen, J., Zhan, W., Rao, Y., 2014b. A simple error estimation method for linear-regression-based thermal sharpening techniques with the consideration of scale difference. Geo Spatial Inf. Sci. 17 (1), 54–59. https://doi.org/10.1080/10095020.2014.889546.
Chybicki, A., Łubniewski, Z., 2017. Optimized AVHRR land surface temperature downscaling method for local scale observations: case study for the coastal area of the Gulf of Gdańsk. Open Geosci. 9, 419–435. https://doi.org/10.1515/geo-2017-0032.
Coll, C., Caselles, V., Galve, J.M., Valor, E., Niclòs, R., Sánchez, J.M., Rivas, R., 2005. Ground measurements for the validation of land surface temperatures derived from AATSR and MODIS data. Rem. Sens. Environ. 97, 288–300.
Deng, C., Wu, C., 2013a. Examining the impacts of urban biophysical compositions on surface urban heat island: a spectral unmixing and thermal mixing approach. Rem. Sens. Environ. 131, 262–274.
Deng, C., Wu, C., 2013b. Estimating very high resolution urban surface temperature using a spectral unmixing and thermal mixing approach. Int. J. Appl. Earth Obs. Geoinf. 23, 155–164.
Dominguez, A., Kleissl, J., Luvall, J.C., Rickman, D.L., 2011. High-resolution urban thermal sharpener (HUTS). Rem. Sens. Environ. 115, 1772–1780. https://doi.org/10.1016/j.rse.2011.03.008.
Dozier, J., 1981. A method for satellite identification of surface temperature fields of subpixel resolution. Rem. Sens. Environ. 11, 221–229.
Duan, S.B., Li, Z.L., 2016. Spatial downscaling of MODIS land surface temperatures using geographically weighted regression: case study in Northern China. IEEE Trans. Geosci. Rem. Sens. 54 (11), 6458–6469.
Ebrahimy, H., Azadbakht, M., 2019. Downscaling MODIS land surface temperature over a heterogeneous area: an investigation of machine learning techniques, feature selection, and impacts of mixed pixels. Comput. Geosci. 124, 93–102. https://doi.org/10.1016/j.cageo.2019.01.004.
Essa, W., Verbeiren, B., van der Kwast, J., Van de Voorde, T., Batelaan, O., 2012. Evaluation of the DisTrad thermal sharpening methodology for urban areas. Int. J. Appl. Earth Obs. Geoinf. 19, 163–172. https://doi.org/10.1016/j.jag.2012.05.010.
Eswar, R., Sekhar, M., Bhattacharya, B.K., 2016. Disaggregation of LST over India: comparative analysis of different vegetation indices. Int. J. Rem. Sens. 37 (5), 1035–1054. https://doi.org/10.1080/01431161.2016.1145363.
Fassnacht, K.S., Gower, S.T., Mackenzie, M.D., Nordheim, E.V., Lillesand, T.M., 1997. Estimating the leaf area index of north central Wisconsin forests using the Landsat Thematic Mapper. Rem. Sens. Environ. 61, 229–245.
Gao, F., Masek, J., Schwaller, M., Hall, F., 2006. On the blending of the Landsat and MODIS surface reflectance: predicting daily Landsat surface reflectance. IEEE Trans. Geosci. Rem. Sens. 44 (8), 2207–2218.
Gao, F., Kustas, W.P., Anderson, M.C., 2012. A data mining approach for sharpening thermal satellite imagery over land. Rem. Sens. 4, 3287–3319. https://doi.org/10.3390/rs4113287.
Gao, L., Zhan, W., Huang, F., Quan, J., Lu, X., Wang, F., Ju, W., Zhou, J., 2017. Localization or globalization? Determination of the optimal regression window for disaggregation of land surface temperature. IEEE Trans. Geosci. Rem. Sens. 55 (1), 477–490.
Garrigues, S., Allard, D., Baret, F., Weiss, M., 2006a. Quantifying spatial heterogeneity at the landscape scale using variogram models. Rem. Sens. Environ. 103, 81–96.
Garrigues, S., Allard, D., Baret, F., 2006b. Influence of the spatial heterogeneity on the nonlinear estimation of Leaf Area Index from moderate resolution remote sensing data. Rem. Sens. Environ. 106, 286–298.
Garrigues, S., Allard, D., Baret, F., Morisette, J., 2008. Multivariate quantification of landscape spatial heterogeneity using variogram models. Rem. Sens. Environ. 112, 216–230.
Ghosh, A., Joshi, P.K., 2014. Hyperspectral imagery for disaggregation of land surface temperature with selected regression algorithms over different land use land cover scenes. ISPRS J. Photogrammetry Remote Sens. 96, 76–93.
Guillevic, P.C., Privette, J.L., Coudert, B., Palecki, M.A., Demarty, J., Ottlé, C., Augustine, A., 2012. Land Surface Temperature product validation using NOAA's surface climate observation networks-Scaling methodology for the Visible Infrared Imager Radiometer Suite (VIIRS). Rem. Sens. Environ. 124, 282–298.
Guo, L.J., Moore, J.M.M., 1998. Pixel block intensity modulation: adding spatial detail to TM band 6 thermal imagery. Int. J. Rem. Sens. 19, 2477–2491.
Guo, G., Wu, Z., Chen, Y., 2014. Estimation of subpixel land surface temperature using Landsat TM imagery: a case examination over a heterogeneous urban area. In: 2014 Second International Workshop on Earth Observation and Remote Sensing Applications. IEEE Xplore. 2014.
Guo, Q., Pu, R., Li, J., Cheng, J., 2017. A weighted normalized difference water index for water extraction using landsat imagery. Int. J. Rem. Sens. 38 (19), 5430–5445.
Gustafson, W.T., Handcock, R., Gillespie, A.R., Tonooka, H., 2003. An image-sharpening method to recover stream temperatures from ASTER images. Remote Sensing for Environmental Monitoring, GIS Applications, and Geology II. In: Ehlers, Manfred (Ed.), Proc. SPIE 4886, 72–83.
He, C., Shi, P., Xie, D., Zhao, Y., 2010. Improving the normalized difference built-up index to map urban built-up areas using a semiautomatic segmentation approach. Remote Sensing Letters 1 (4), 213–221.
Herrero-Huerta, M., Lagüela, S., Alfieri, S.M., Menenti, M., 2019. Generating high-temporal and spatial resolution TIR image data. Int. J. Appl. Earth Obs. Geoinf. 78, 149–162. https://doi.org/10.1016/j.jag.2019.01.016.
Hu, Y., Zhou, X., Zhang, Y., 2021. Subpixel temperature estimation by information transfer with adaptive ensemble extreme learning machine (IT-AEELM). IEEE J. Sel. Top. Appl. Earth Obs. Rem. Sens. 14, 6743. https://doi.org/10.1109/JSTARS.2021.3091125.
Huang, B., Wang, J., Song, H., Fu, D., Wong, K., 2013. Generating high spatiotemporal resolution land surface temperature for urban heat island monitoring. Geosci. Rem. Sens. Lett. IEEE 10 (5), 1011–1015. https://doi.org/10.1109/LGRS.2012.2227930.
Huete, A.R., 1988. A soil adjusted vegetation index (SAVI). Rem. Sens. Environ. 25, 295–309.
Hutengs, C., Vohland, M., 2016. Downscaling land surface temperatures at regional scales with random forest regression. Rem. Sens. Environ. 178, 127–141.
Inamdar, A.K., French, A., 2009. Disaggregation of GOES land surface temperatures using surface emissivity. Geophys. Res. Lett. 36, L02408. https://doi.org/10.1029/2008GL036544.

Inamura, M., 1993. Spatial resolution improvement of a low spatial resolution image using spatial component extracted from high spatial resolution images. In: IEEE International Geoscience and Remote Sensing Symposium. IGARSS, pp. 2105–2107. https://doi.org/10.1109/IGARSS.1993.3220381993.
Jeganathan, C., Hamm, N.A.S., Mukherjee, S., Atkinson, P.M., Raju, P.L.N., Dadhwal, V.K., 2011. Evaluating a thermal image sharpening model over a mixed agricultural landscape in India. Int. J. Appl. Earth Obs. Geoinf. 13 (2), 178–191.
Jiang, Y., Weng, Q., 2013. Estimating LST using a vegetation-cover-based thermal sharpening technique. Geosci. Rem. Sens. Lett. IEEE 10 (5), 1249–1252. https://doi.org/10.1109/LGRS.2013.2257667.
Jiang, Y., Fu, P., Weng, Q., 2015. Downscaling GOES land surface temperature for assessing heat wave health risks. Geosci. Rem. Sens. Lett. IEEE 12 (8), 1605–1609. https://doi.org/10.1109/LGRS.2015.2414897.
Kallel, A., Ottlé, C., Hégarat-Mascle, S.L., Maignan, F., Courault, D., 2013. Surface temperature downscaling from multiresolution instruments based on markov models. IEEE Trans. Geosci. Rem. Sens. 51 (3), 1588–1612. https://doi.org/10.1109/TGRS.2012.2207461.
Keramitsoglou, I., Kiranoudis, C.T., Weng, Q., 2013. Downscaling geostationary land surface temperature imagery for urban analysis. Geosci. Rem. Sens. Lett. 10 (5), 1253–1257. https://doi.org/10.1109/LGRS.2013.2257668.
Kustas, W.P., Norman, J.M., Anderson, M.C., French, A.N., 2003. Estimating subpixel surface temperatures and energy fluxes from the vegetation index–radiometric temperature relationship. Remote Sens. Environ. 85, 429–440.
Li, Z.-L., Tang, B.-H., Wu, H., Ren, H., Yan, G., Wan, Z., Trigo, I.F., Sobrino, J.A., 2013. Satellite-derived land surface temperature: current status and perspectives. Rem. Sens. Environ. 131, 14–37. https://doi.org/10.1016/j.rse.2012.12.008.
Li, X., Xin, X., Jiao, J., Peng, Z., Zhang, H., Shao, S., Liu, Q., 2017. Estimating subpixel surface heat fluxes through applying temperature-sharpening methods to MODIS data. Rem. Sens. 9, 836. https://doi.org/10.3390/rs9080836.
Li, W., Nic, L., Li, Z.-L., Wu, H., 2018. Downscaling Land Surface Temperature by Using Random Forest Regression Algorithm, pp. 2527–2530. IGARSS 2018, IEEE Xplore.
Li, W., Wu, H., Duan, S.-B., Li, Z.-L., Liu, Q., 2019. Selection of predictor variables in downscaling land surface temperature using random forest algorithm. IGARSS 2019, 1817–1820. . IEEE Xplore.
Li, H., Wu, G., Xu, F., Li, S., 2021. Landsat-8 and Gaofen-1 image-based inversion method for the downscaled land surface temperature of rare earth mining areas. Infrared Phys. Technol. 113, 103658. https://doi.org/10.1016/j.infrared.2021.103658.
Li, N., Wu, H., Ouyang, X., 2022. Localized Downscaling of Urban Land Surface Temperature—A Case Study in Beijing, China. Rem. Sens. 14, 2390. https://doi.org/10.3390/rs14102390.
Liang, L., Li, J., Chen, Y., Xia, H., Chen, Q., 2021. An auto-adjusted kernel method for thermal sharpening with local and object-based window strategies. IEEE J. Sel. Top. Appl. Earth Obs. Rem. Sens. 14, 3659–3668. https://doi.org/10.1109/JSTARS.2021.3067349.
Lillesand, T.M., Kiefer, R.W., Chipman, J.W., 2008. Remote Sensing and Image Interpretation, sixth ed. John Wiley and Sons Inc, New York, p. 359.
Lillo-Saavedra, M., García-Pedrero, A., Merino, G., Gonzalo-Martín, C., 2018. TS^{2}uRF: a new method for sharpening thermal infrared satellite imagery. Rem. Sens. 10, 249. https://doi.org/10.3390/rs10020249.
Liu, D., Pu, R., 2008. Downscaling thermal infrared radiance for subpixel land surface temperature retrieval. Sensors 8 (4), 2695–2706.
Liu, K., Su, H., 2016. Enhancing the spatial resolution of satellite-derived land surface temperature (LST) using an operational trapezoid interpolation disaggregation model (OTI_DisTrad). In: Fourth International Workshop on Earth Observation and Remote Sensing Applications 978-1-5090-1479-8/16/$31.00 ©2016 IEEE. IEEE Xplore, p. 5. 2016.
Liu, H., Weng, Q., 2018. Scaling effect of fused ASTER-MODIS land surface temperature in an urban environment. Sensors 18, 4058. https://doi.org/10.3390/s18114058.
Liu, D., Zhu, X., 2012. An enhanced physical method for downscaling thermal infrared radiance. Geosci. Rem. Sens. Lett. IEEE 9, 690–694.
Liu, K., Su, H., Li, X., 2016. Estimating high-resolution urban surface temperature using a hyperspectral thermal mixing (HTM) approach. IEEE J. Sel. Top. Appl. Earth Obs. Rem. Sens. 9 (2), 804–815. . 0.1109/JSTARS.2015.2459375.
Liu, K., Su, H., Li, X., Chen, S., Zhang, R., Wang, W., Yang, L., Liang, H., Yang, Y., 2018. A thermal disaggregation model based on trapezoid interpolation. IEEE J. Sel. Top. Appl. Earth Obs. Rem. Sens. 11 (3), 808–820. https://doi.org/10.1109/JSTARS.2018.2790002.
Liu, K., Su, H., Tian, J., Li, X., Wang, W., Yang, L., Liang, H., 2018b. Assessing a scheme of spatial-temporal thermal remote-sensing sharpening for estimating regional evapotranspiration. Int. J. Rem. Sens. 39 (10), 3111–3137. https://doi.org/10.1080/01431161.2018.1434326.
Liu, X., Wang, Y., Liu, Q., 2018c. PSGAN: a generative adversarial network for remote sensing image pan-sharpening. In: Proc. Of 25th IEEE International Conference on Image Processing (ICIP), 7–10, pp. 873–877. https://doi.org/10.1109/ICIP.2018.8451049Athens, Greece, Oct.
Liu, K., Wang, S., Li, X., Wu, T., 2019. Spatially disaggregating satellite land surface temperature with a nonlinear model across agricultural areas. J. Geophys. Res.: Biogeosciences 124 (11), 3232–3251.
Luo, X., Chen, Y., Wang, Z., Li, H., Peng, Y., 2021. Spatial downscaling of MODIS land surface temperature based on a geographically and temporally weighted autoregressive model. IEEE J. Sel. Top. Appl. Earth Obs. Rem. Sens. 14, 7637–7653. https://doi.org/10.1109/JSTARS.2021.3094184.
Ma, J., Zhang, W., Marinoni, A., Gao, L., Zhang, B., 2016. An improved spatial and temporal reflectance unmixing model to synthesize time series of Landsat-like images. Rem. Sens. 10, 1388.
Maeda, E.E., 2014. Downscaling MODIS LST in the East African mountains using elevation gradient and land-cover information. Int. J. Rem. Sens. 35 (9), 3094–3108. https://doi.org/10.1080/01431161.2014.903442.
Mahour, M., Tolpekin, V., Stein, A., Sharifi, A., 2017. A comparison of two downscaling procedures to increase the spatial resolution of mapping actual evapotranspiration. ISPRS J. Photogrammetry Remote Sens. 126, 56–67. https://doi.org/10.1016/j.isprsjprs.2017.02.004.
Mao, Q., Peng, J., Wang, Y., 2021. Resolution enhancement of remotely sensed land surface temperature: current status and perspectives. Rem. Sens. 13, 1306. https://doi.org/10.3390/rs13071306.
Matson, M., Dozier, J., 1981. Identification of subresolution high temperature sources using a thermal IR sensor. Photogramm. Eng. Rem. Sens. 47 (9), 1311–1318.
McFeeters, S., 1996. The use of the Normalized Difference Water Index (NDWI) in the delineation of open water features. Int. J. Rem. Sens. 17, 1425–1432.
Mechri, R., Ottlé, C., Pannekoucke, O., Kallel, A., 2014. Genetic particle filter application to land surface temperature downscaling. J. Geophys. Res. Atmos. 119, 2131–2146. https://doi.org/10.1002/2013JD020354.
Mechri, R., Ottlé, C., Pannekoucke, O., Kallel, A., Maignan, F., Courault, D., Trigo, I.F., 2016. Downscaling Meteosat land surface temperature over a heterogeneous landscape using a data assimilation approach. Rem. Sens. 8, 586. https://doi.org/10.3390/rs8070586.
Mitraka, Z., Chrysoulakis, N., Doxani, G., Frate, F.D., Berger, M., 2015. Urban surface temperature time series estimation at the local scale by spatial-spectral unmixing of satellite observations. Rem. Sens. 7, 4139–4156. https://doi.org/10.3390/rs70404139.
Mohamadi, B., Chen, S., Balz, T., Gulshad, K., McClure, S.C., 2019. Normalized method for land surface temperature monitoring on coastal reclaimed areas. Sensors 19 (22), 4836.
Moosavi, V., Talebi, A., Mokhtari, M.H., Shamsi, S.R.F., Niazi, Y., 2015. A wavelet-artificial intelligence fusion approach (WAIFA) for blending Landsat and MODIS surface temperature. Rem. Sens. Environ. 169, 243–254. https://doi.org/10.1016/j.rse.2015.08.015.
Mukherjee, S., Joshi, P., Garg, R., 2014. A comparison of different regression models for downscaling Landsat and MODIS land surface temperature images over heterogeneous landscape. Adv. Space Res. 54, 655–669. https://doi.org/10.1016/j.asr.2014.04.013.
Mukherjee, S., Joshi, P.K., Garg, R.D., 2015. Regression-kriging technique to downscale satellite-derived land surface temperature in heterogeneous agricultural landscape. IEEE J. Sel. Top. Appl. Earth Obs. Rem. Sens. 8 (3), 1245–1250. https://doi.org/10.1109/JSTARS.2015.2396032. 3. .
Nichol, J., 2009. An emissivity modulation method for spatial enhancement of thermal satellite images in urban heat island analysis. Photogramm. Eng. Rem. Sens. 75 (5), 547–556.
Nishii, R., Kusanobu, S., Tanaka, S., 1996. Enhancement of low spatial resolution image based on high resolution bands. IEEE Trans. Geosci. Rem. Sens. 34 (5), 1151–1158.
Njuki, S.M., Mannaerts, C.M., Su, Z., 2020. An improved approach for downscaling coarse-resolution thermal data by minimizing the spatial averaging biases in random forest. Rem. Sens. 12, 3507. https://doi.org/10.3390/rs12213507.

Olivera-Guerra, L., Mattar, C., Merlin, O., Durán-Alarcón, C., Santamaría-Artigas, A., Fuster, R., 2017. An operational method for the disaggregation of land surface temperature to estimate actual evapotranspiration in the arid region of Chile. ISPRS J. Photogrammetry Remote Sens. 128, 170–181. https://doi.org/10.1016/j.isprsjprs.2017.03.014.

Peng, Y., Li, W., Luo, X., Li, H., 2019. A geographically and temporally weighted regression model for spatial downscaling of MODIS land surface temperatures over urban heterogeneous regions. IEEE Trans. Geosci. Rem. Sens. 57 (7), 5012–5027.

Pereira, O.J.R., Melfi, A.J., Montes, C.R., Lucas, Y., 2018. Downscaling of ASTER thermal images based on geographically weighted regression kriging. Rem. Sens. 10, 633. https://doi.org/10.3390/rs10040633.

Pu, R., 2021. Assessing scaling effect in downscaling land surface temperature in a heterogenous urban environment. Int. J. Appl. Earth Obs. Geoinf. 96, 102256. https://doi.org/10.1016/j.jag.2020.102256.

Pu, R., Bonafoni, S., 2021. Reducing scaling effect on downscaled land surface temperature maps in heterogenous urban environments. Rem. Sens. 13 (24), 5044. https://doi.org/10.3390/rs13245044. 2021, 25 pp.

Pu, R., Bonafoni, S., 2022. Correcting scaling effect in downscaling surface temperature at high resolutions with a multiple regional correction approach. Geosci. Rem. Sens. Lett. IEEE 19, 1–5. https://doi.org/10.1109/LGRS.2022.3186467. 2022. .

Qian, L., Cui, H., 2008. Relationship between normalized difference moisture index and land surface temperature. Geogr. Res. 27 (6), 1358–1367.

Qiu, J., Yang, J., Wang, Y., Su, H., 2018. A comparison of NDVI and EVI in the DisTrad model for thermal sub-pixel mapping in densely vegetated areas: a case study in Southern China. Int. J. Rem. Sens. 39 (8), 2105–2118.

Quan, J., Zhan, W., Ma, T., Du, Y., Guo, Z., Qin, B., 2018. An integrated model for generating hourly landsat-like land surface temperatures over heterogeneous landscapes. Remote Sens. Environ. 206, 403–423.

Rouse, J.W., Haas, R.H., Schell, J.A., Deering, D.W., 1973. Monitoring vegetation systems in the great plains with ERTS. Proc. Third ERTS Symp. 1, 48–62.

Sattari, F., Hashim, M., Pour, A.B., 2018. Thermal sharpening of land surface temperature maps based on the impervious surface index with the TsHARP method to ASTER satellite data: a case study from the metropolitan Kuala Lumpur, Malaysia. Measurement 125, 262–278. https://doi.org/10.1016/j.measurement.2018.04.092.

Sharma, K.V., Khandelwal, S., Kaul, N., 2020. Downscaling of coarse resolution land surface temperature through vegetation indices based regression models. In: Ghosh, J.K., da Silva, I. (Eds.), Applications of Geomatics in Civil Engineering, Lecture Notes in Civil Engineering, 33. https://doi.org/10.1007/978-981-13-7067-0_51.

Sismanidis, P., Keramitsoglou, I., Kiranoudis, C.T., 2015. Evaluating the operational retrieval and downscaling of urban land surface temperatures. Geosci. Rem. Sens. Lett. IEEE 12 (6), 1312–1316. https://doi.org/10.1109/LGRS.2015.2397450.

Sismanidis, P., Keramitsoglou, I., Kiranoudis, C.T., Bechtel, B., 2016. Assessing the capability of a downscaled urban land surface temperature time series to reproduce the spatiotemporal features of the original data. Rem. Sens. 8, 274. https://doi.org/10.3390/rs8040274.

Sismanidis, P., Keramitsoglou, I., Bechtel, B., Kiranoudis, C.T., 2017. Improving the downscaling of diurnal land surface temperatures using the annual cycle parameters as disaggregation kernels. Rem. Sens. 9, 23. https://doi.org/10.3390/rs9010023.

Snyder, W.C., Wan, Z., Zhang, Y., Feng, Y.Z., 1997. Requirements for satellite land surface temperature validation using a silt playa. Rem. Sens. Environ. 61, 279–289.

Sobrino, J.A., Romaguera, M., 2004b. Land surface temperature retrieval from MSG1-SEVIRI data. Rem. Sens. Environ. 92, 247–254.

Sobrino, J.A., Oltra-Carrió, R., Sòria, G., Bianchi, R., Paganini, M., 2012. Impact of spatial resolution and satellite overpass time on evaluation of the surface urban heat island effects. Remote Sens. Environ. 117, 50–56. 2012.

Stathopoulou, M., Cartalis, C., 2009. Downscaling AVHRR land surface temperatures for improved surface urban heat island intensity estimation. Rem. Sens. Environ. 112, 2592–2605.

Tom, V.T., Carlotto, M.J., Scholten, D.K., 1985. Spatial sharpening of Thematic Mapper data using a multiband approach. Opt. Eng. 24 (6), 1026–1029.

Tuia, D., Pacifici, F., Kanevski, M., Emery, W.J., 2009. Classification of very high spatial resolution imagery using mathematical morphology and support vector machines. IEEE Trans. Geosci. Rem. Sens. 47, 3866–3879. https://doi.org/10.1109/TGRS.2009. 2027895.

Vaculik, A.F., Bah, A.R., Norouzi, H., Beale, C., Valentine, M., Ginchereau, J., Blake, R., 2019. Downscaling of satellite land surface temperature data over urban environments. IGARSS. . 2019, IEEE Xplore.

Van Leeuwen, W.J.D., Huete, A.R., 1996. Effects of standing litter on the biophysical interpretation of plant canopies with spectral indices. Rem. Sens. Environ. 55 (2), 123–138.

Wan, Z., Dozier, J., 1996. A generalized split-window algorithm for retrieving land-surface temperature from space. IEEE Trans. Geosci. Rem. Sens. 34 (4), 892–905.

Wang, L., Qu, J.J., 2007. NMDI: a normalized multi-band drought index for monitoring soil and vegetation moisture with satellite remote sensing. Geophys. Res. Lett. 34, L20405. https://doi.org/10.1029/2007GL031021.

Wang, Z., Sun, Y., Ren, H., Qin, Q., Han, G., 2017. Downscaling Research of Remotely Sensed Land Surface Temperature. IGARSS. 2017, 2017 IEEE Xplore.

Wang, J., Schmitz, O., Lu, M., Karssenberg, D., 2020. Thermal unmixing based downscaling for fine resolution diurnal land surface temperature analysis. ISPRS J. Photogrammetry Remote Sens. 161, 76–89.

Wang, R., Gao, W., Peng, W., 2020b. Downscale MODIS land surface temperature based on three different models to analyze surface urban heat island: a case study of Hangzhou. Rem. Sens. 12, 2134. https://doi.org/10.3390/rs12132134.

Wang, J.W., Chow, W.T.L., Wang, Y.-C., 2020c. A global regression method for thermal sharpening of urban land surface temperatures from MODIS and Landsat. Int. J. Rem. Sens. 41 (8), 2986–3009. https://doi.org/10.1080/01431161.2019.1697009.

Weng, Q., Fu, P., 2014. Modeling diurnal land temperature cycles over Los Angeles using downscaled GOES imagery. ISPRS J. Photogrammetry Remote Sens. 97, 78–88. https://doi.org/10.1016/j.isprsjprs.2014.08.009.

Weng, Q., Fu, P., Gao, F., 2014. Generating daily land surface temperature at Landsat resolution by fusing Landsat and MODIS data. Rem. Sens. Environ. 145, 55–67.

White-Newsome, J.L., Brines, S.J., Brown, D.G., Dvonch, J.T., Gronlund, C.J., Zhang, K., Oswald, E.M., O'Neill, M.S., 2013. Validating satellite-derived land surface temperature with *in situ* measurements: a public health perspective. Environ. Health Perspect. 12 (8), 925–931.

Wu, H., Li, W., 2019. Downscaling land surface temperatures using a random forest regression model with multitype predictor variables. IEEE Access 7, 21904–21916. https://doi.org/10.1109/ACCESS.2019.2896241.

Wu, M.Q., Niu, Z., Wang, C.Y., Wu, C.Y., Wang, L., 2012. Use of MODIS and Landsat time series data to generate high-resolution temporal synthetic Landsat data using a spatial and temporal reflectance fusion model. J. Appl. Remote Sens. 6 (1), 063507.

Wu, M., Li, H., Huang, W., Niua, Z., ang, C., 2015. Generating daily high spatial land surface temperatures by combining ASTER and MODIS land surface temperature products for environmental process monitoring. Environ. Sci.: Process. Impacts 17, 1396–1404. https://doi.org/10.1039/c5em00254k.

Wu, J., Zhong, B., Tian, S., Yang, A., Wu, J., 2019. Downscaling of urban land surface temperature based on multi-factor geographically weighted regression. J. Selected Topics Appl. Earth Observ. Rem. Sens. 12 (8), 2897–2911. https://doi.org/10.1109/JSTARS.2019.2919936.

Xia, H., Chen, Y., Zhao, Y., Chen, Z., 2018. Regression-then-fusion" or "fusion-then-regression"? a theoretical analysis for generating high spatiotemporal resolution land surface temperatures. Rem. Sens. 10, 1382. https://doi.org/10.3390/rs10091382.

Xia, H., Chen, Y., Li, Y., Quan, J., 2019. Combining kernel-driven and fusion-based methods to generate daily high spatial resolution land surface temperatures. Rem. Sens. Environ. 224, 259–274.

Xia, H., Chen, Y., Quan, J., Li, J., 2019b. Object-based window strategy in thermal sharpening. Rem. Sens. 11, 634.

Xu, H., 2008. A new index for delineating built-up land features in satellite imagery. Int. J. Rem. Sens. 29 (14), 4269–4276.

Xu, J., Zhang, F., Jiang, H., Hu, H., Zhong, K., Jing, W., Yang, J., Jia, B., 2020. Downscaling ASTER land surface temperature over urban areas with machine learning-based area-to-point regression kriging. Rem. Sens. 12, 1082. https://doi.org/10.3390/rs12071082.

Xu, S., Zhao, Q., Yin, K., He, G., Zhang, Z., Wang, G., Wen, Zhang, N., 2021. Spatial downscaling of land surface temperature based on a multi-factor geographically weighted machine learning model. Rem. Sens. 13, 1186. https://doi.org/10.3390/rs13061186.

Xue, J., Leung, Y., Fung, T., 2019. An unmixing-based Bayesian model for spatio-temporal satellite image fusion in heterogeneous landscapes. Rem. Sens. 11, 324.

Yang, G.J., Pu, R.L., Zhao, C.J., Huang, W.J., Wang, J.H., 2011. Estimation of subpixel land surface temperature using an endmember index based technique: a case examination on ASTER and MODIS temperature products over a heterogeneous area. Rem. Sens. Environ. 115 (5), 1202–1219.

Yang, Y., Cao, C.X., Li, X., Zhu, X., 2017. Downscaling land surface temperature in an arid area by using multiple remote sensing indices with random forest regression. Rem. Sens. 9, 789. https://doi.org/10.3390/rs9080789.
Yang, C., Zhan, Q., Lv, Y., Liu, H., 2019. Downscaling land surface temperature using multiscale geographically weighted regression over heterogeneous landscapes in Wuhan, China. J. Selected Topics Appl. Earth Observ. Rem. Sens. 12 (12), 5213–5222. https://doi.org/10.1109/JSTARS.2019.2955551.
Yang, J., Yao, Y., Wei, Y., Zhang, Y., Jia, K., Zhang, X., Shang, K., Bei, X., Guo, X., 2020. A robust method for generating high-spatiotemporal-resolution surface reflectance by fusing MODIS and Landsat data. Rem. Sens. 12, 2312.
Yao, Y., Chang, C., Ndayisaba, F., Wang, S., 2020. A new approach for surface urban heat island monitoring based on machine learning algorithm and spatiotemporal fusion model. IEEE Access 164268, 164281. https://doi.org/10.1109/ACCESS.2020.3022047.
Yin, Z., Wu, P., Foody, G.M., Wu, Y., Liu, Z., Du, Y., Ling, F., 2021. Spatiotemporal fusion of land surface temperature based on a convolutional neural network. Trans. Geosci. Rem. Sens. 59 (2), 1808–1822. https://doi.org/10.1109/TGRS.2020.2999943.
Yoo, C., Im, J., Park, S., Cho, D., 2020. Spatial downscaling of MODIS land surface temperature: recent research trends, challenges, and future directions. Kor. J. Rem. Sens. 36 (4), 609–626. https://doi.org/10.7780/kjrs.2020.36.4.9.
Zakšek, K., Oštir, K., 2012. Downscaling land surface temperature for urban heat island diurnal cycle analysis. Rem. Sens. Environ. 117, 114–124.
Zakšek, K., Schroedter-Homscheidt, M., 2009. Parameterization of air temperature in high temporal and spatial resolution from a combination of the SEVIRI and MODIS instruments. ISPRS J. Photogrammetry Remote Sens. 64, 414–421. https://doi.org/10.1016/j.isprsjprs.2009.02.006.
Zawadzka, J., Corstanje, R., Harris, J., Truckell, I., 2020. Downscaling Landsat-8 land surface temperature maps in diverse urban landscapes using multivariate adaptive regression splines and very high resolution auxiliary data. Int. J. Digital Earth 13 (8), 899–914. https://doi.org/10.1080/17538947.2019.1593527.
Zha, Y., Gao, J., Ni, S., 2003. Use of normalized difference built-up index in automatically mapping urban areas from TM imagery. Int. J. Rem. Sens. 24 (3), 583–594. https://doi.org/10.1080/01431160304987.
Zhai, H., Huang, F., Qi, H., 2020. Generating high resolution LAI based on a modified FSDAF model. Rem. Sens. 12, 150.
Zhan, W., Chen, Y., Zhou, J., Li, J., Liu, W., 2011. Sharpening thermal imageries: a generalized theoretical framework from an assimilation perspective. Trans. Geosci. Rem. Sens. 49 (2), 773–789.
Zhan, W., Chen, Y., Wang, J., Zhou, J., Quan, J., Liu, W., Li, J., 2012. Downscaling land surface temperatures with multi-spectral and multi-resolution images. Int. J. Appl. Earth Obs. Geoinf. 18, 23–36. https://doi.org/10.1016/j.jag.2012.01.003.
Zhan, W., Chen, Y., Zhou, J., Wang, J., Liu, W., Voogt, J., Zhu, X., Quan, J., Li, J., 2013. Disaggregation of remotely sensed land surface temperature: literature survey, taxonomy, issues, and caveats. Remote Sens. Environ. 131, 119–139. https://doi.org/10.1016/j.rse.2012.12.014.
Zhang, T., Huang, X., Wen, D., Li, J., 2017. Urban building density estimation from high- resolution imagery using multiple features and support vector regression. IEEE J. Sel. Top. Appl. Earth Obs. Rem. Sens. 10, 3265–3280. https://doi.org/10.1109/JSTARS.2017.2669217.
Zhang, X., Zhao, H., Yang, J., 2019. Spatial downscaling of land surface temperature in combination with TVDI and elevation. Int. J. Rem. Sens. 40 (5–6), 1875–1886. https://doi.org/10.1080/01431161.2018.1489164.
Zhang, H., Song, Y., Han, C., Zhang, L., 2021. Remote sensing image spatiotemporal fusion using a generative adversarial network. Trans. Geosci. Rem. Sens. 59 (5), 4273. https://doi.org/10.1109/TGRS.2020.3010530. 2486. .
Zhou, X., Zhang, Y., 2021. Ensemble extreme learning machine approach to thermal infrared subpixel temperature estimation. Geosci. Rem. Sens. Lett. IEEE 18 (5), 920–923. https://doi.org/10.1109/LGRS.2020.2985500.
Zhou, J., Liu, S., Li, M., Zhan, W., Xu, Z., Xu, T., 2016. Quantification of the scale effect in downscaling remotely sensed land surface temperature. Rem. Sens. 8, 975. https://doi.org/10.3390/rs8120975.
Zhou, D., Xiao, J., Bonafoni, S., Berger, C., Deilami, K., Zhou, Y., Frolking, S., Yao, R., Qiao, Z., Sobrino, J., 2019. Satellite remote sensing of surface urban heat islands: progress, challenges, and perspectives. Rem. Sens. 11 (1), 48. https://doi.org/10.3390/rs11010048.
Zhu, X.L., Chen, J., Gao, F., Chen, X.H., Masek, J.G., 2010. An enhanced spatial and temporal adaptive reflectance fusion model for complex heterogeneous regions. Remote Sens. Environ. 114, 2610–2623.
Zhu, X.L., Helmer, E.H., Gao, F., Liu, D.S., Chen, J., Lefsky, M.A., 2016. A flexible spatiotemporal method for fusing satellite images with different resolutions. Remote Sens. Environ. 172, 165–177.
Zhu, X., Cai, F., Tian, J., Williams, T., 2018. Spatiotemporal fusion of multisource remote sensing data: literature survey, taxonomy, principles, applications, and future directions. Rem. Sens. 10, 527.
Zhu, S., Liu, Y., Hua, J., Zhang, G., Zhou, Y., Xiang, J., 2018b. Monitoring spatio-temporal variance of an extreme heat event using multiple-source remote sensing data. Chin. Geogr. Sci. 28 (5), 744–757. https://doi.org/10.1007/s11769-018-0989-8.